Università degli Studi di Firenze

DOTTORATO DI RICERCA IN
"*Ingegneria Dei Sistemi Elettronici*"

CICLO XXV

COORDINATORE Prof. Tortoli Piero

Linear Feature Extraction from High-Resolution SAR Images

Settore Scientifico Disciplinare ING-INF/01

Dottorando
Dott. Fabbrini Luca

Tutore
Prof. Pieraccini Massimiliano

Anni 2010/2012

To Giulia and Luna,
who differently,
have made it possible.

Abstract

The raising availability of Synthetic Aperture Radar (SAR) images makes it possible to acquire and add important information to the one obtained via the classical optical domain. Nevertheless, SAR images are not so easy to interpret because they are subjected to distortions (i.e. foreshortening, layover, and radar shadows) and they show a disturbance usually referred as multiplicative speckle noise.

In an automatic image interpretation system, the accurate extraction of the main features, which are present on the acquired scene, is usually the most fundamental step to deal with. In this context, linear feature extraction plays an important role for a fully automatic image understanding system.

In this thesis, linear feature extraction issue is firstly tackled by detecting amplitude discontinuities (i.e. edges) of the signal. Next, the obtained result is refined by an edge linking stage so that, finally, the boundary of the object of interest is extracted throughout a higher-level model.

Exploiting the speckle model in the edge detector operation, the knowledge of the probability density function (pdf) of the filtered data is used to obtain a desired probability of false alarms (PFA) at the output of the system. In this context, both parametric and non-parametric statistical edge detectors are evaluated on high-resolution SAR images. Next, presupposing classical assumptions on the distribution of such images, a novel statistical model is devised to cope with the final pdf of general linear filtered data. Even though the presented model is an approximation of the real pdf that does not have closed form, it fits well the data and its mathematical treatability enable us to exploit the model in different way, even improving the performance of the subsequent linking stage.

To free the processing by statistical assumptions of data, general multiscale linear filtering is investigated. Several methods of scale combinations and automatic thresholding are evaluated to obtain an improvement on the final edge detection performance.

The edge linking stage presented in this thesis makes use of the sequential edge linking (SEL) algorithm already known in literature, which models the linking issue as a shortest path problem (SPP). Nevertheless, the application of the original method to the one-look SAR data shows many problems and drawbacks. For this reason, two novel SPP metrics have been proposed and new steps have been added to the original algorithm. Following the study on the edge detection, both a parametric and a non-parametric metric has been proposed to make the method generally applicable. Furthermore, exploiting the model developed for the edge detection, we proved the useful of its application in improving SEL performance.

The algorithm devised to extract linear features (e.g. roads and runways), relies on the Hough Transform framework and tries reconstructing the object boundaries as composition of linear segments. In particular, in the extraction step, the road is recognized as composition of regions that are limited by parallel lines and characterized by a low radar cross section (RCS) due to a high homogeneous material. Moreover, to study the loss of information occurring in the discretization of the Hough Transform definition, new theoretical bounds on the parameter sampling have been obtained and compared with their signal processing counterpart.

Finally, to improve edge detection performance and approach a higher level of processing, a novel despeckling algorithm is presented. It belongs to the class of non-linear, anisotropic diffusion filters that apply a partial differential equation (PDE) onto the image in analysis. In particular, since the proposed filter is a PDE-based filter, no noise model is presupposed so that, in principle, it can be applied to any noise type. Consequently, no statistical modeling effort is required to change sensor or data type (e.g. intensity or amplitude). Ultimately, since the application of the proposed despeckled filter enables a straightforward segmentation to be applied, even on one-look Cosmo-SkyMed images, such approach extends the extraction of a possible general shaped feature.

Acknowledgment

I would like to thank every people who have been part of this Ph.D. thesis, both directly and indirectly. In particular, I am surely indebted to my supervisor at IDS Company, Dr. Gianpaolo Pinelli, who addressed this thesis for what it is now.

Then, I would like to thank all the colleagues (and friends at the same time) at the Signature Technology Laboratory of the IDS Radar Division, who have supported my efforts by offering invaluable coffees and suggestions. Among these, special thanks go to Ing. Marco Messina, my desktop mate, who has the gift of the gab (even though not often), and who shared with me a very joyful conference to DLR, in the easy-pronunciation city of Oberpfaffenhofen.

A final thank goes to Prof. Massimiliano Pieraccini and Prof. Carlo Atzeni, my supervisors at Florence University.

Contents

Introduction

In the last years, synthetic aperture radar (SAR) images have become always more and more available. Especially for the satellite SAR system, the revisit time is always lower and the same area can be acquired more times in a day. The huge amount of information stored in such data asks a raising need of automatic algorithms, which could applied to such images routinely, or they could provide a useful support to the human image interpretation.

Unfortunately, SAR images suffer from many distortions due to the acquisition system technique. This fact, in addition to the developed custom of analyzing erroneously SAR images as it was its optic counterpart, makes the need of automatic methods of fundamental importance on SAR images. Nevertheless, the presence of such distortions does not enable the application of classic algorithms to be performed directly. Hence, new tools and algorithms have to be devised specifically for SAR environment.

Motivation and Problem Statement

In an automatic interpretation system, the scene under analysis is usually decomposed in several features, which could be extracted separately or jointly, and from which the original scene semantic can be retrieved when they are joined together as in the original image. Focusing the attention on the singular feature extraction, such a processing step is usually composed by different layers, every one belonging to a different processing scale. In particular, there is often a low-level processing useful to extract the different parts of the object under analysis. Subsequently, a higher-level step assembles such parts to verify if they can inch (or not) a specific prior model.

In the context of linear feature extraction, a novel processing chain that manages to perform both low-level task (edge detection) and high-level step (road/runway extraction) is presented in this thesis.

Outline

In order to face a greater number of cases than possible, we propose both statistical and multiscale edge detection. Moreover, even in the subsequent step of refining the resulting edge map, both parametric and non-parametric techniques are developed. Finally, considering linearizing even smooth curves by composition of small segments, an extraction algorithm relying on the Hough Transform framework has been devised, see Fig. I for a sample results.

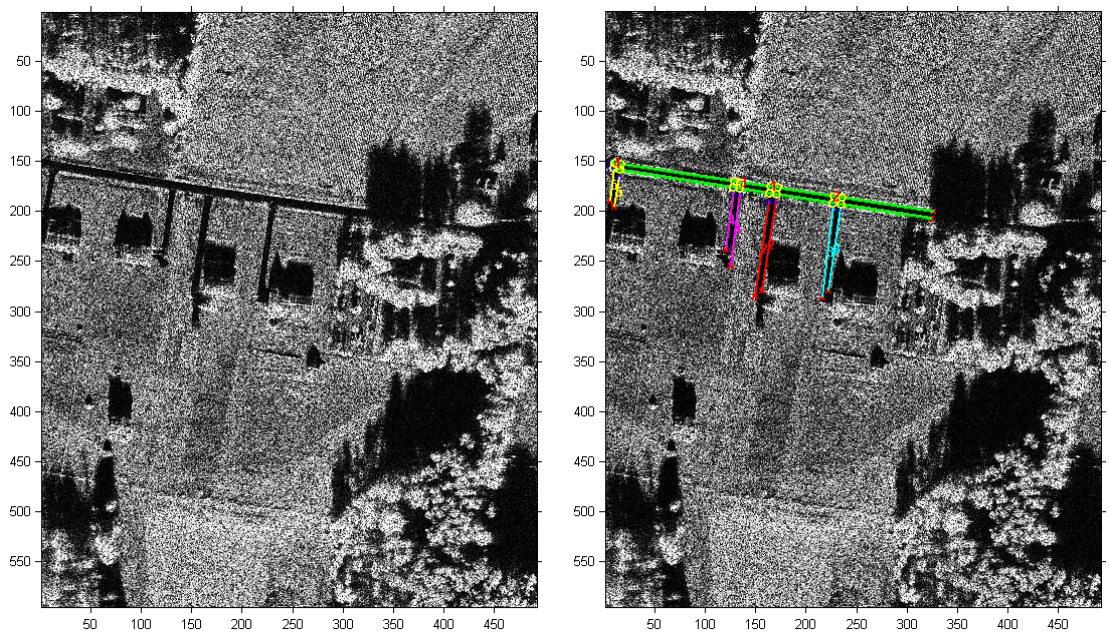

Fig. I - Road extraction from a SAR image acquired by an airborne radar sensor (MSTAR dataset). Lines of the same color indicate the same road part. Yellow dots indicates the crossroad points.

Finally, both to extend the range of application of the proposed processing chain and to improve the final performance, a novel despeckling filter has been conceived, see Fig. II. It belongs to the PDE-based filter class and can be applied to any noise type (not only speckle).

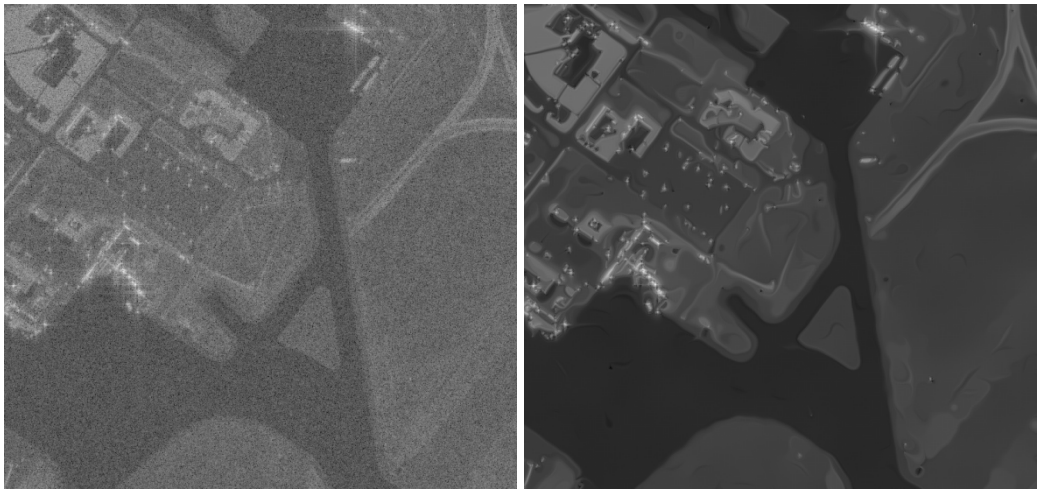

(a)

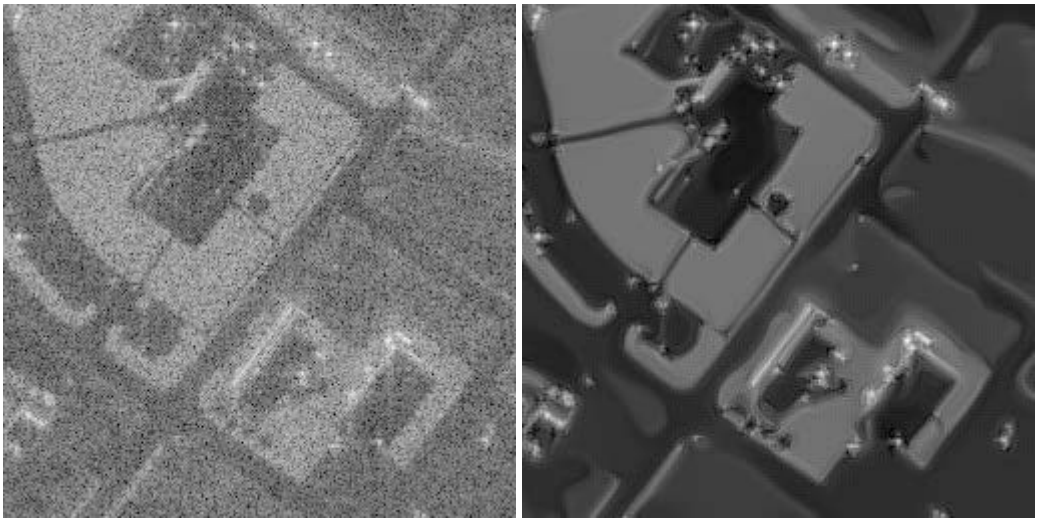

(b)

Fig. II - Despeckling results on a one-look CSK image acquired over Tucson (Arizona) - Courtesy of ASI.
(a) Whole image (on the left) and its despeckled version by the proposed algorithm (on the right).
(b) Respective image magnification around airport buildings.

Chapter 1

Synthetic Aperture Radar (SAR) Systems

Fundamentally, the radar principle exploits the physics behavior of electromagnetic waves, i.e. that part of the power emitted by a source hits a material and comes back (backscattered) toward the source itself. The received signal, once analyzed, makes it possible to detect, locate and even characterize the hit material. For this reasons, remote surveillance of sensible areas was one of the first military applications of the radar technique. Usually, in this case, a continuously rotating antenna was used to detect and measure the distance of an object from the radar one circular sector at time (see Fig. 1.1). Clearly, the distance measurements are done exploiting the delay of the received echo, since that, given a target at distance d from the radar, the relative echo is received after the time $t = 2d/c$, with c the wave propagation velocity in the vacuous. Moreover, an important property for these radars was the capacity to distinguish between two objects (resolution) that are close in the direction of range (wave propagation) or in direction of the antenna scanning (azimuth). At first glance, the range resolution can be expressed as the minimum range distance between two objects that enables the relative echoes to be received separately. In this case the well-known **range resolution** formula is:

$$r_d = c\tau/2 \tag{1.1}$$

with r_d the range resolution and τ the duration of the transmitted impulse. Instead, the azimuth resolution relies on the angle at $-3dB$ (β_{az}) of the antenna pattern in that direction, which is proportional to the dimension D of the antenna itself (considering aperture antenna) that is often expressed as:

$$\beta_{az} \approx \lambda/D \tag{1.2}$$

and from the object distance d. In particular, the **azimuth resolution** r_{az} can be expressed as the footprint of the antenna at distance d:

$$r_{az} = \beta_{az} d \approx \frac{\lambda}{D}\, d \tag{1.3}$$

Whereas in surveillance radars the image formation depends on the rotation of the system, other type of radar imagery can be obtained with the movement of a platform bearing a fixed side-looking antenna (Fig. 1.2).

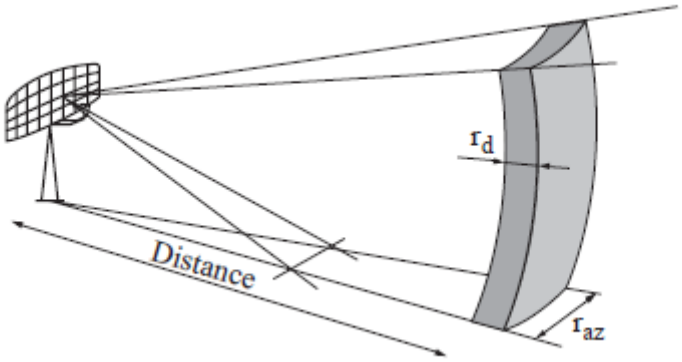

Fig. 1.1 - Resolution cell of a surveillance radar.

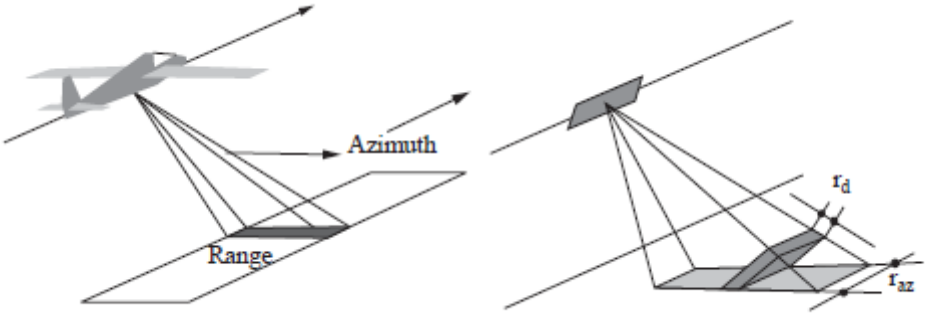

Fig. 1.2 - Airborne radar system and its resolution cell.

This operating principle, which is known as side-looking airborne radars (SLAR), was widely used for many years, largely for military cartography purposes. The width of the image acquired in range direction is usually called swath and two points, namely near and far range, limit it. As can be seen from Fig. 1.3, the range resolution r_d correspond to a different value r_g when it is projected to the ground (ground resolution). Even though the ground resolution r_g geometrically depend on the range position of the echo between the near and far range, the **ground resolution** of the image is usually considered fixed and equal to the one of the central echo:

$$r_g = \frac{c\tau}{2\sin\vartheta} \tag{1.4}$$

where ϑ is the incidence angle.

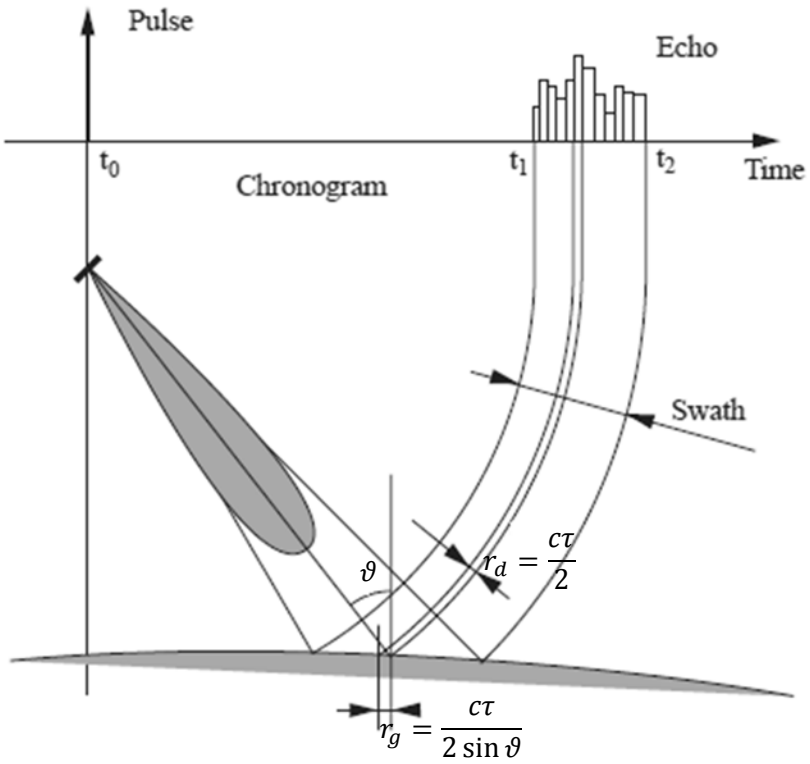

Fig. 1.3 - Range resolution cell of a surveillance radar.

Commonly to all radar systems, the real range resolution gets worse when the effect of the matched filter used in reception is considered. In particular, considering an ideal matched filter of the transmitted signal, the range resolution doubles ($r_d = c\tau$) so that a modulation of the signal (pulse compression) is usually considered before transmitting. In this field, one of the most used compression techniques is surely the chirp modulation, where the frequency of the signal is varied linearly in time. Consider transmitting the signal in Fig. 1.4, which can be mathematically written as:

$$S_T(t) = A\cos\left(\omega_0 t + \frac{1}{2}Kt^2\right)\mathrm{rect}\left(\frac{t-\tau/2}{\tau}\right) \tag{1.5}$$

with K the chirp rate (usually in the order of 10^{13}). In this case its instantaneous phase and frequency are:

$$\begin{aligned} \Phi(t) &= \omega_0 t + \frac{1}{2}Kt^2 \\ f(t) &= \frac{1}{2\pi}\Phi'(t) = f_0 + \frac{Kt}{2\pi} \end{aligned} \tag{1.6}$$

so that the price to be paid from the compression it is the greater bandwidth of the signal that now spans on a frequency interval of width about $\Delta f = Kt/2\pi$.

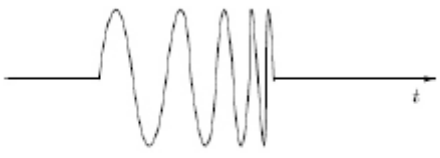

Fig. 1.4 - Pulse with chirp modulation.

Nevertheless, applying the matched filter to this signal, its output (time up to the first null) endures only for a time interval of $\Delta t = 2\pi/K\tau$ so that, with respect to τ (duration of the exit without modulation), there is the following **range resolution gain**:

$$G_{r_d} = \frac{c\tau}{c\Delta t} = \frac{K\tau^2}{2\pi} \tag{1.7}$$

For example, in the case of Cosmo-SkyMed (CSK) Spotlight 2 mode, we have a range chirp rate $K = 2.7 \cdot 10^{12}$, chirp duration $\tau = 75\mu s$, and therefore a gain $G_{r_d} \approx 2417$. Usually, since the chirp bandwidth Δf can be considered as an intrinsic system parameter, the range resolution is sometimes expressed by it:

$$r_d = c\Delta t = \frac{c}{\Delta f} = \frac{c}{2(\Delta f)_{Eq}} \tag{1.8}$$

where $(\Delta f)_{Eq}$ is the equivalent chirp bandwidth, sometimes approximated as:

$$(\Delta f)_{Eq} = K\tau \tag{1.9}$$

Finally, for the sake of completeness, it is helpful to point out that the *rect* function in Eq. (1.5) is nearly never used. In fact, it does have the shortest main lobe extend in frequency domain (therefore the minimum extent of the main bandwidth), but it also spreads too much energy on its sidelobes. For this reason, to reduce sidelobe effects at expense of resolution, the *rect* function in Eq. (1.5) is usually replaced by an appropriate weighting function (e.g. Hamming function) [1].

1.1 SAR Principle

In the real aperture radar (RAR) system, the azimuth resolution r_{az} is very different from the one obtained in range. Considering the parameters of the SAR CSK system in Spotlight 2 mode, the maximum equivalent chirp bandwidth is $(\Delta f)_{Eq} = 400MHz$ and corresponds to a ground resolution of $r_g \approx 1m$ even with very steep incidence angles $\vartheta = 20°$. Instead, exploiting only the real aperture of the radar in azimuth (see Eq. (1.3)), considering the carriage frequency $f_0 = 9.6GHz$, the antenna length $D = 5.6m$, an orbital height of $h = 619.6km$ and an incidence angle $\vartheta = 20°$, the azimuth resolution of the RAR CSK system would be:

$$r_{az} = \beta_{az} d = \frac{\lambda}{D} \frac{h}{\cos\vartheta} \approx 367km \tag{1.10}$$

In order to obtain a better azimuth resolution, an antenna of length L, with L greater than the actual length D, can be artificially synthetized. The idea underlying this synthetic length is very simple and at the same time very powerful. Let us also assume that the radar transmits a pulse each time it travels the distance r_{az}, with r_{az} being less than L. If the distance r_{az} is considerably less than L, a point target P is illuminated by several pulses as the radar instrument passes over. The number of these pulses will be equal to the ratio L/r_{az}. The target P will thus contribute to each of these pulses by returning an echo composed of an amplitude and a phase. Differently from the amplitude, the phase is strongly affected by the wave's round trip between the radar and the target. Each time the wave travels one wavelength, its phase completes a full cycle. In fact, whereas each pulse to which P contributes will have approximately the same amplitude, the phase of each pulse will be offset by a great amount. Thus, the solution is to modify the phase of the samples to which the target P has contributed, so that they all have the same phase and can be added together without cancellations. Moreover, after this phase compensation helpful to focalize the contributions from P, the echoes received from the other targets near P will have a phase that span from all its range $[-\pi, \pi]$, so that in the final sum there will be many cancellation effects and their final contribute will be nearly negligible.

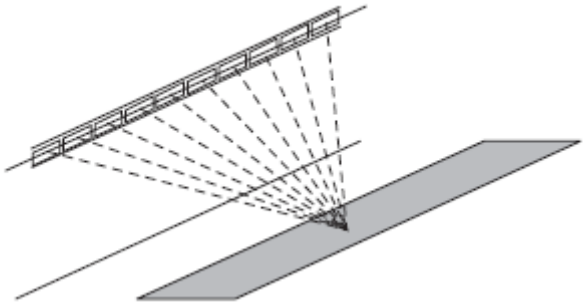

Fig. 1.5 - Synthetic aperture principle: along its path the radar acquires a series of images that are combined by post processing. The final image looks like an image acquired by the antenna sum of all the basic ones.

A first practical approach to retrieve the azimuth resolution through the synthetic aperture method is to consider the image as it was acquired by an array antenna (Fig. 1.5). In this case, the array elements are simply composed by the positions of the real antenna (of length $\ll L$) when the pulses were transmitted. When an array antenna of length L is taken into account, the $-3dB$ angle β'_{az} in that direction becomes $\beta'_{az} \approx \lambda/L$, whereas the same angle for the single element would be $\beta_{az} \approx \lambda/D$. However, indicating with d the distance target-antenna and inserting in the array formulas the fact that electromagnetic waves cross a distance $2d$ from their phase reference, the angle β'_{az} simply becomes [1]:

$$\beta'_{az} \approx \frac{\lambda}{2L} \tag{1.11}$$

Now, exploiting very simple considerations (Fig. 1.6) of the acquisition geometry, we can see that the synthetized length can be expressed as (in the case of small β_{az}):

$$L = 2\tan\left(\frac{\beta_{az}}{2}\right)d \approx \beta_{az}d \tag{1.12}$$

Therefore, the final **azimuth resolution** will be:

$$r_{az} = \beta'_{az}d = \frac{\lambda}{2L}d = \frac{\lambda}{2\beta_{az}d}d = \frac{\lambda}{2(\lambda/D)d}d \tag{1.13}$$

that with simplifications is:

$$r_{az} = \frac{D}{2} \tag{1.14}$$

For example, with an antenna length $D = 5.6m$ (CSK system) the final azimuth resolution would be $r_{az} = 2.8m$.

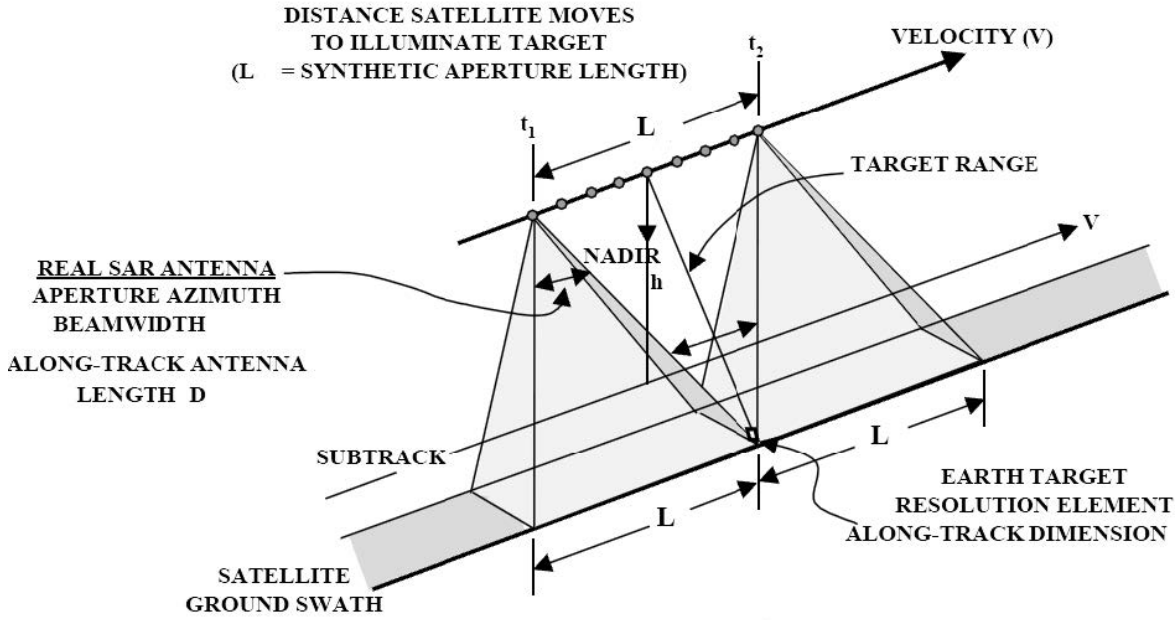

Fig. 1.6 - Acquisition geometry of the SAR system.

After a first intuitive approach, a more analytical formulation of the SAR principle could be formulated. From the acquisition geometry of Fig. 1.7, considering transmitting the signal $S_T(t)$ (here modulation is neglected since it is used only for range resolution purpose), whose complex expression could be written as $S_T(t) = e^{j\omega_0 t}$, the signal received by the radar could be expressed, at a first approximation, as the sum of the echoes from the P_k point targets alone:

$$S_R(t) = \sum_k A_k \, e^{j\varphi_k} e^{j\omega_0\left(t-\frac{2R_k(t)}{c}\right)} = e^{j\omega_0 t} \sum_k V_k \, e^{-j\frac{4\pi}{\lambda}R_k(t)} \tag{1.15}$$

with V_k composed by the received attenuated amplitude A_k (it also takes into account the antenna pattern coefficients in azimuth direction) and the so called "natural" phase of the targets φ_k, which indicates how the dielectric or geometric properties of the target can interact with the wave. For each reception, the processing matched to the target P_1 implies a multiplication of $S_R(t)$ with the phase term relative to P_1, so that after the processing we have:

$$S_{R_1}(t) = S_R(t) e^{j\frac{4\pi}{\lambda}R_1(t)} = e^{j\omega_0 t} \sum_k V_k \, e^{-j\frac{4\pi}{\lambda}[R_k(t)-R_1(t)]} \tag{1.16}$$

Clearly, from the acquisition geometry we have (exploiting also Taylor approximation):

$$\begin{aligned} R_1(t) &= \sqrt{R_0^2 + (vt)^2} \approx R_0\left(1 + \frac{(vt)^2}{2R_0^2}\right) \\ R_k(t) &= \sqrt{R_0^2 + (vt - x_k)^2} \approx R_0\left(1 + \frac{v^2(t-t_k)^2}{2R_0^2}\right) \end{aligned} \tag{1.17}$$

where $x_k = vt_k$ is the distance P_1 - P_k and t_k is the time when the radar sees P_k at a range R_0 (also called point of approach). Exploiting Eq. (1.17) and matching at each reception the phase of P_1, the phase relative to P_k changes with the time (i.e. it changes at each reception). In fact, indicating the round trip difference between P_k and P_1 as $\Delta R_k(t) = R_k(t) - R_1(t)$, we have:

$$\Delta\Phi_k(t) = \frac{4\pi}{\lambda}\Delta R_k(t) \approx \frac{2\pi\left(x_k^2 - 2x_k\, vt\right)}{\lambda R_0^2} \tag{1.18}$$

so that, in the final sum, the phase term of the echo k will have assumed all the values between π and $-\pi$.

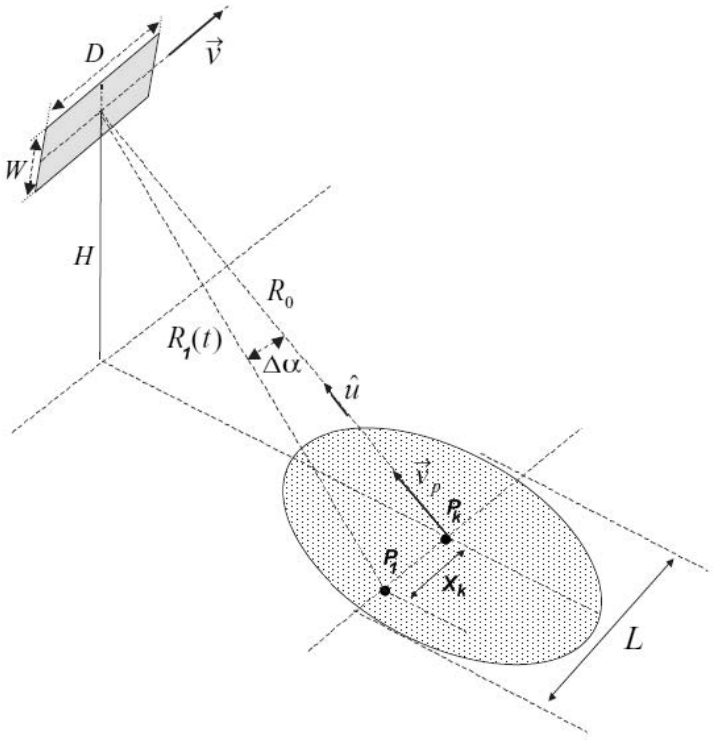

Fig. 1.7 - Along track SAR geometry.

The previous discussion is a general analytical consideration to make the SAR principle clearer, but a more formal treatment is required to understand the involved variables. Let k be the index of the points acquired by the radar for a given range (see Fig. 1.8), r_{az} the azimuth distance separating each point, and i the index of the point at the center of the antenna pattern (i.e. the index of the point of approach), and k' the index of the point inside the antenna footprint.

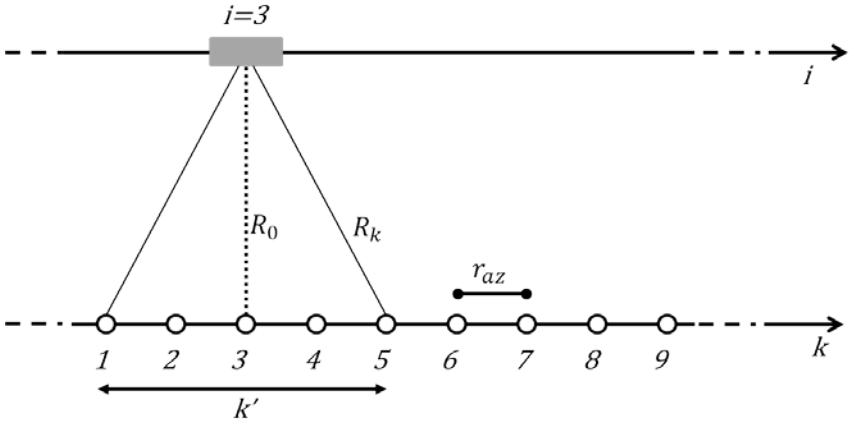

Fig. 1.8 - Along track SAR geometry reference system.

Considering the processing always matched to the point of approach i (as happens in the real case), the phase difference of any point k at distance $r_{az}(k-i)$ from the point i (which is at distance R_0 from the antenna) after the matching with i is:

$$\Delta\Phi_{k,i} = \frac{4\pi}{\lambda}[R_k - R_0] \approx \frac{2\pi r_{az}^2 (k-i)^2}{\lambda R_0} = \Delta\Phi([k-i]^2) \tag{1.19}$$

with:

$$R_k = \sqrt{R_0^2 + r_{az}^2 (k-i)^2} \approx R_0 \left(1 + \frac{r_{az}^2 (k-i)^2}{2R_0^2}\right) \tag{1.20}$$

where the dependence of the phase difference from the square of the index difference is highlighted. Then, the received signal from each point k' inside the antenna footprint of i can be written as:

$$S(i) = \sum_{k'=i-\frac{N}{2}}^{i+\frac{N}{2}} \beta(k'-i)\, e^{j\Delta\Phi\left([k'-i]^2\right)} \tag{1.21}$$

where $\beta(n)$ are the antenna pattern coefficients in azimuth direction with only N coefficients different from 0. For example, if during the acquisition we had collected only one response $S(i)$ and we would see the final value of the pixel around the point of index k, we have to adjust the phase from $S(i)$ to match the point with index k:

$$S_f(k) = S(i)e^{-j\Delta\Phi([k-i]^2)} = \sum_{k'=i-\frac{N}{2}}^{i+\frac{N}{2}} \beta(k'-i)\, e^{j\left\{\Delta\Phi\left([k'-i]^2\right)-\Delta\Phi([k-i]^2)\right\}} \tag{1.22}$$

Now, if k was the index at distance n from i, we would have:

$$S_f(k) = S(i)e^{-j\Delta\Phi(n^2)} = \sum_{k'=i-\frac{N}{2}}^{i+\frac{N}{2}} \beta(k'-i)\, e^{j\left\{\Delta\Phi\left([k'-i]^2\right)-\Delta\Phi(n^2)\right\}} \tag{1.23}$$

Clearly, in Eq. (1.23) the matched point $k' = k = i + n$ has a phase difference equal to zero and the received amplitude is multiplied by $\beta(n)$. Always from Eq. (1.23), we can see that a point at distance d from k (i.e. posing $k' = k + d = i + n + d$ in Eq. (1.23)) would give a contribution to the final response of k equal to:

$$\beta(n+d)e^{j\{\Delta\Phi([n+d]^2)-\Delta\Phi(n^2)\}} = \beta(n+d)e^{j\Delta\Phi(n^2+2nd)} \tag{1.24}$$

Hence, not only does this contribution depends from the distance d from k, but even from the distance between k and i expressed by n. Now, as in the real case, considering to form the response of the point k by a collection of N responses $S(i)$ ($N/2$ at the left of k and $N/2$ at the right), we have:

$$S_f(k) = \sum_{i=k-\frac{N}{2}}^{k+\frac{N}{2}} S(i)\, e^{-j\Delta\Phi([k-i]^2)} = \sum_{i=k-\frac{N}{2}}^{k+\frac{N}{2}} \sum_{k'=i-\frac{N}{2}}^{i+\frac{N}{2}} \beta(k'-i)\, e^{j\left\{\Delta\Phi\left([k'-i]^2\right)-\Delta\Phi([k-i]^2)\right\}} \tag{1.25}$$

Therefore, a point at distance d from k (i.e. $k' = k + d$) would give a contribution:

$$\begin{aligned} S_f(k) &= \sum_{i=k-\frac{N}{2}}^{k+\frac{N}{2}} S(i)\, e^{-j\Delta\Phi([k-i]^2)} = \sum_{i=k-\frac{N}{2}}^{k+\frac{N}{2}} \beta(k+d-i)e^{j\{\Delta\Phi([k+d-i]^2)-\Delta\Phi([k-i]^2)\}} \\ &= \sum_{i=k-\frac{N}{2}}^{k+\frac{N}{2}} \beta(k+d-i)e^{j\{\Delta\Phi(d^2+2kd-2di)\}} \end{aligned} \tag{1.26}$$

From Eq. (1.26), for a general point at distance d from k (i.e. fixing d and k in Eq. (1.26)), we can see how the phase contribution depends on i:

$$\sum_{i=k-\frac{N}{2}}^{k+\frac{N}{2}} e^{j\{\Delta\Phi(-2di)\}} = \sum_{i=k-\frac{N}{2}}^{k+\frac{N}{2}} e^{-j\frac{2\pi r_{az}^2 2di}{\lambda R_0}} = \sum_{i=k-\frac{N}{2}}^{k+\frac{N}{2}} e^{-j\frac{2\pi di}{N_a}} \tag{1.27}$$

with $N_a = \lambda R_0/2r_{az}^2$ the so called "azimuth compression rate". Therefore, as said before, for a point target at distance d from the reference point k, varying i (i.e. during the acquisition time) the phase contribution spans regularly between π and $-\pi$, so nullifying the final contribution, see Fig. 1.9.

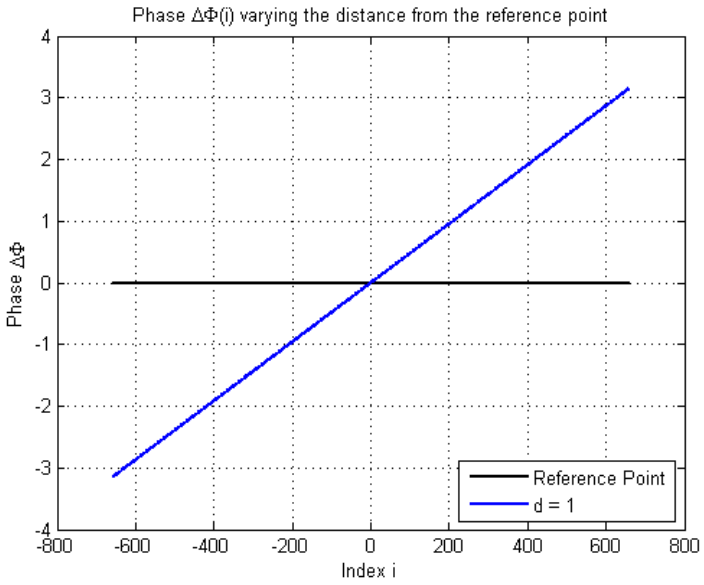

Fig. 1.9 - Phase contributions of the reference point and of the point at distance $d = 1$ from it, varying the point of approach expressed by the index i.

An interesting thing is to see the instantaneous frequency (brought the received signal in base band) of each echo during the illumination time (also called dwell or integration time). From Eq. (1.17) we have:

$$f_1(t) = -\frac{\Phi_1'(t)}{2\pi} = -\frac{2}{\lambda}R_1'(t) = -\left(\frac{2v^2}{\lambda R_0}\right)t$$
$$f_k(t) = -\frac{\Phi_k'(t)}{2\pi} = -\frac{2}{\lambda}R_k'(t) = -\left(\frac{2v^2}{\lambda R_0}\right)(t - t_k) \quad (1.28)$$

Practically, Eq. (1.28) indicates the Doppler history of each echo that is nothing but a negative slope line function of the time (see Fig. 1.10).

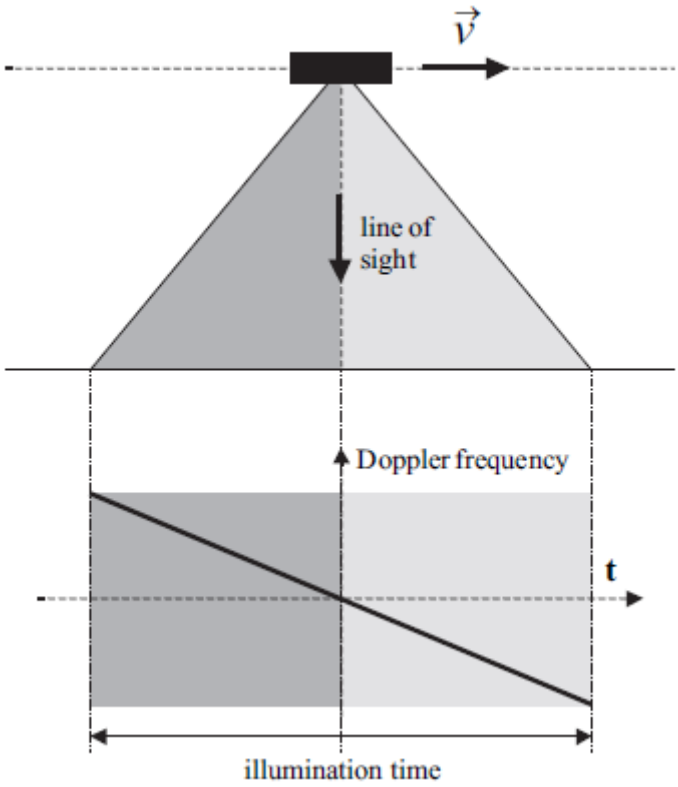

Fig. 1.10 - Doppler history of the central point.

Clearly, from Eq. (1.28), the Doppler history of all points P_k acquired by the radar during the illumination time of P_1 are lines with the same negative slope of P_1 but with a different offset $f_\Delta = 2v^2 t_k/\lambda R_0$. In fact, indicating with $B_D = 2f_{D_M}$ the Doppler bandwidth of the system and with T_0 the illumination time of P_1, the whole Doppler situation can be depicted as in Fig. 1.11.

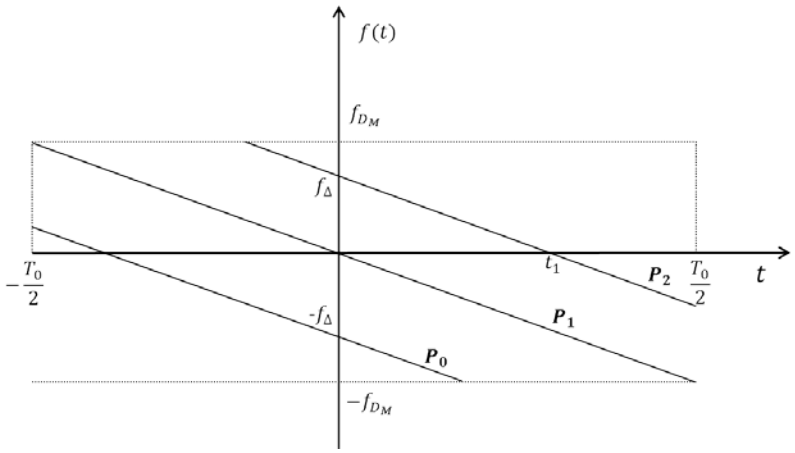

Fig. 1.11 - Doppler history of all the points illuminated during P_1 acquisition.

1.2 Mobile Target Effects

Until now, we have considered fixed target points during the illumination time. Nevertheless, when this hypothesis is not respected, the final effect is simply a shift in the azimuth value of these targets. Intuitively, if a target P_1 is mobile and moves towards the radar, it will add a phase change that it will not be taken into account in the previous model. In particular, there will be a point P_k on the same range as P_1whose phase distribution will be precisely that of "mobile P_1". In this case, mobile P_1 will be correctly processed by the phase distribution planned for P_k. Therefore, after the processing, P_1 will be placed in the same position of P_k (see Fig. 1.12).

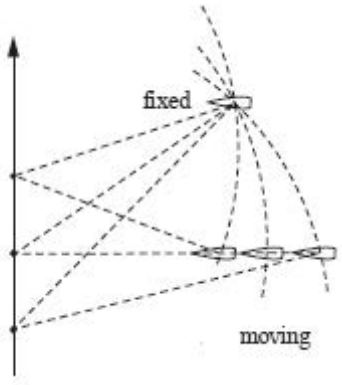

Fig. 1.12 - Moving ship in the same range cell of a fixed one. The moving ship is seen by the radar equally to the fixed one, even though the latter is several azimuth cell away from the former.

Analytically, considering the configuration of Fig. 1.7, the range of the point P_1 could be written as $R_1(t) = R_F(t) + R_M(t)$, with $R_F(t)$ the range considering the point fixed (zero mobility), and $R_M(t)$ the contribute due to the mobility. Therefore, the phase shift of the point P_1 when P_k has a range R_0 is:

$$\Delta\Phi_k(t) = \frac{4\pi}{\lambda}[R_1(t) - R_k(t)] = \frac{4\pi}{\lambda}[\Delta R_k(t) + R_M(t)] \approx \frac{2\pi v^2 t^2}{\lambda R_0} + \frac{4\pi v_p t}{\lambda} \tag{1.29}$$

where we have presupposed the point P_1 with a **constant radial velocity** $v_p = R'_M(t)$. Therefore, the relative shift Doppler added to Eq. (1.29) is:

$$\Delta\Phi_k(t) \approx \frac{2\pi v^2 t^2}{\lambda R_0} + \frac{4\pi v_p t}{\lambda} = \frac{2\pi v^2}{\lambda R_0}\left[\left(t + R_0\frac{v_p}{v^2}\right)^2 - R_0^2\frac{v_p^2}{v^4}\right] \tag{1.30}$$

that is a Doppler history:

$$\Delta f_k(t) = -\frac{\Delta\Phi_k'(t)}{2\pi} \approx -\frac{2v^2}{\lambda R_0}\left(t + R_0\frac{v_p}{v^2}\right) \tag{1.31}$$

Thus, from Eq. (1.31) we have a final response as there was a time shift $t_{az} = R_0\frac{v_p}{v^2}$ that correspond to an **azimuth shift** x_{az}:

$$x_{az} = vt_{az} = R_0\frac{v_p}{v} \tag{1.32}$$

For example, the CSK satellite velocity, which was sampled in the middle of an acquisition, has a velocity vector in Earth-Centered, Earth-Fixed (ECEF) Cartesian coordinates (see Fig. 1.13):

$$\boldsymbol{v} = (v_x, v_y, v_z) = (-2171{,}5561, -4812) \tag{1.33}$$

which corresponds to a velocity module $v = |\boldsymbol{v}| = 7667ms^{-1}$. Thus, if we assume the nominal CSK orbital height of $h = 619.6km$, an incidence angle $\vartheta = 20°$, and a ship that goes in the ground range direction at 20 knots, that is $v_g = 10.29\ ms^{-1}$, we have a shift in azimuth of:

$$x_{az} = R_0\frac{v_p}{v} = \frac{h}{\cos\vartheta}\frac{v_g\sin\vartheta}{v} = 302.7m \tag{1.34}$$

where v_p is the range projection of the ship ground range velocity, i.e. $v_p = v_g\sin\vartheta$.

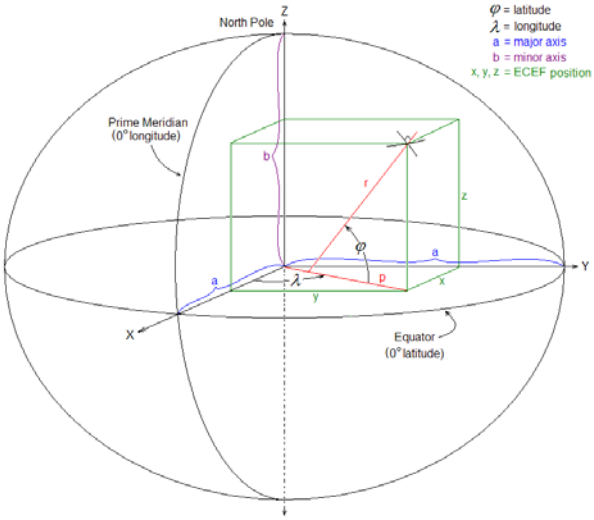

Fig. 1.13 - Earth-Centered, Earth-Fixed (ECEF) Cartesian coordinates reference system.

1.3 SAR Processing

SAR processing (also called focusing) is the transformation of the raw SAR signal data (here considered as a complex signal retrieved by the I and Q branches of the schema in Fig. 1.14) into a spatial image.

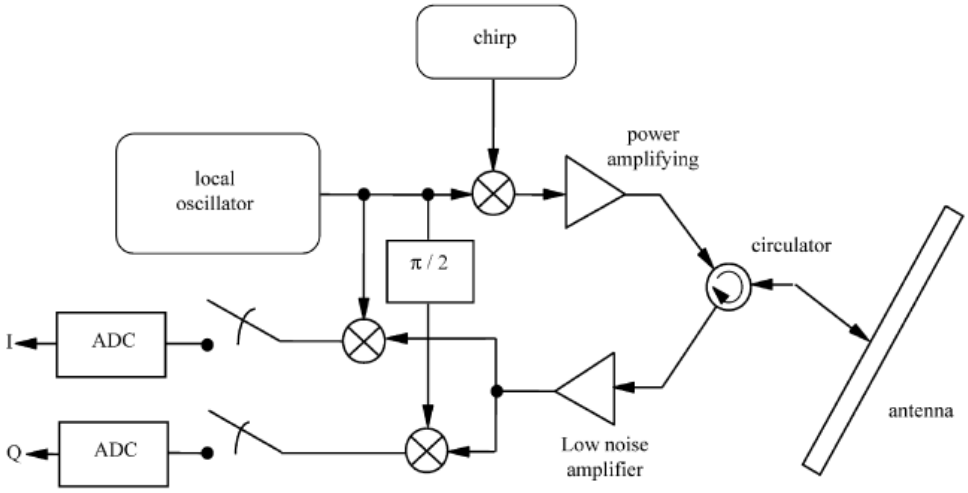

Fig. 1.14 - Block diagram of the radar components.

Ideally, this operation requires the convolution of the raw signal with a two-dimensional space-variant point spread function (PSF) of the SAR data acquisition system. Nevertheless, a full two-dimensional time domain correlator is computationally inefficient and other methods have to be used to perform the focusing operation. One of the first focusing algorithm solving the previous problem was the range-Doppler (RD) algorithm, which takes advantage of fast correlation by using fast Fourier transform (FFT) of the signal. Even though more advanced algorithm has been implemented for focusing purpose [1], the RD still remain a reference since it could be seen as a good trade-off between simplicity and computational efficiency. Basically, considering to transmit the general pulse:

$$S_T(t) = p(t)e^{j\omega_0 t} \tag{1.35}$$

the received echo for a point target located at (x_0, r_0), with x, r respectively the azimuth and range direction, can be written as:

$$S_R(t) = p_R(t - 2R/c)e^{j\omega_0(t-2R/c)} \tag{1.36}$$

where the range R varies with x and it can be expressed as:

$$R(x - x_0, r_0) = \sqrt{{r_0}^2 + (x - x_0)^2} \tag{1.37}$$

As said before, **the range compression** is very easy and it concerns the time reduction of the convolution result between $p_R(t)$ and the appropriate matching filter. Moreover, a range dependent gain correction is applied to the data so that elevation beam pattern and range spreading losses are compensated. Nevertheless, since the PRF is not directly separable as the product of the range and azimuth responses, an intermediate operation has to be done before computing the azimuth compression. In particular, while the sensor passes, a point target located at $x_0 = 0$ and $r = r_0$ has a distance R from the radar that varies as:

$$R(x, r_0) = \sqrt{{r_0}^2 + x^2} \approx r_0 + x^2/2r_0 \tag{1.38}$$

so that, the ensemble of all received echoes referred to it (reported in base band) can be written as:

$$S_R(x, r_0) = e^{-j\omega_0 \frac{2}{c}\Delta R(x, r_0)} \tag{1.39}$$

with $\Delta R(x, r_0)$ the phase difference relative to the its point of approach:

$$\Delta R(x, r_0) = R(x, r_0) - r_0 \approx x^2/2r_0 \tag{1.40}$$

The term in Eq. (1.40), which is sometimes called **range migration** (RM) term, points out that the distance of the target raises varying the azimuth x. However, the unwonted consequence is that the contribution of the received signal is seen by the radar in different range cells during the motion (see Fig. 1.15).

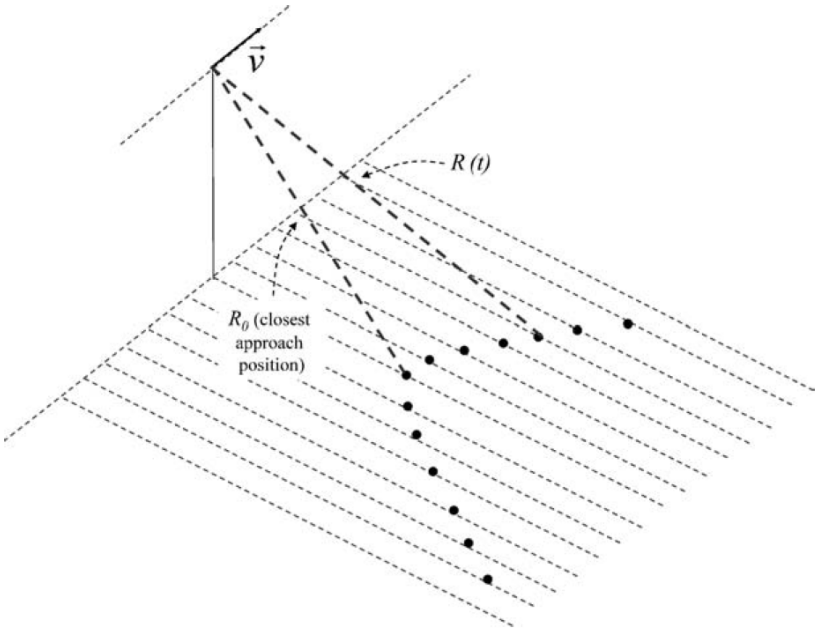

Fig. 1.15 - Range migration effect.

Therefore, the contribution of the target for different pulse transmissions along the azimuth could corresponds to different range cells (greater than the reference range r_0). Consequently, before performing the azimuth compression algorithm, the range cell migration correction (RCMC) has to be performed. Clearly, fixed the pulse repetition frequency (PRF), the RM term is hardly ever an integer multiple of the range resolution, and a time domain interpolation is needed for a fine correction. Then, after the RCMC operation, the phase correction for each azimuth cell takes the name of **azimuth compression** (see Fig. 1.16 for the whole focusing schema).

Sometimes, from a full compressed image in azimuth could be helpful to generate more images with less azimuth resolution. This technique is called **multilooking** and, as we shall see in Chapter 2, it is used to reduce a noiselike disturbance referred as speckle. In this case, after range compression and RCMC, the azimuth frequency spectrum is divided into several portions called looks, where the looks are usually positioned symmetrically around the Doppler centroid frequency (see Fig. 1.17 and Fig. 1.18). The part of the azimuth frequency array for each look is extracted, multiplied by the respective azimuth matched filter frequency response, and the inverse FFT is performed. Then, for each complex image calculated in such a way, the power (also called "intensity") of its complex samples is computed and the final image is generated by the mean of all the previous intensity images. Finally, the square root is often applied to provide data in amplitude format.

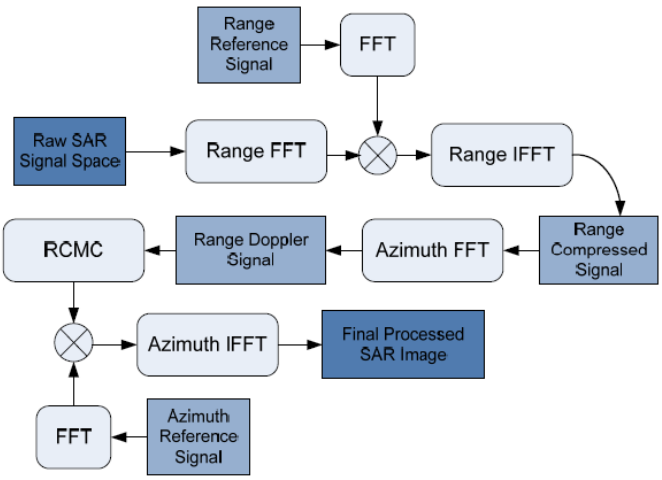

Fig. 1.16 - Block diagram of the range-Doppler focusing algorithm.

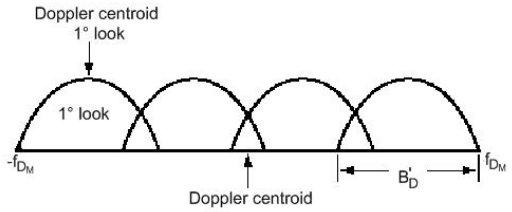

Fig. 1.17 - Multilooking principle: Azimuth frequency spectrum.

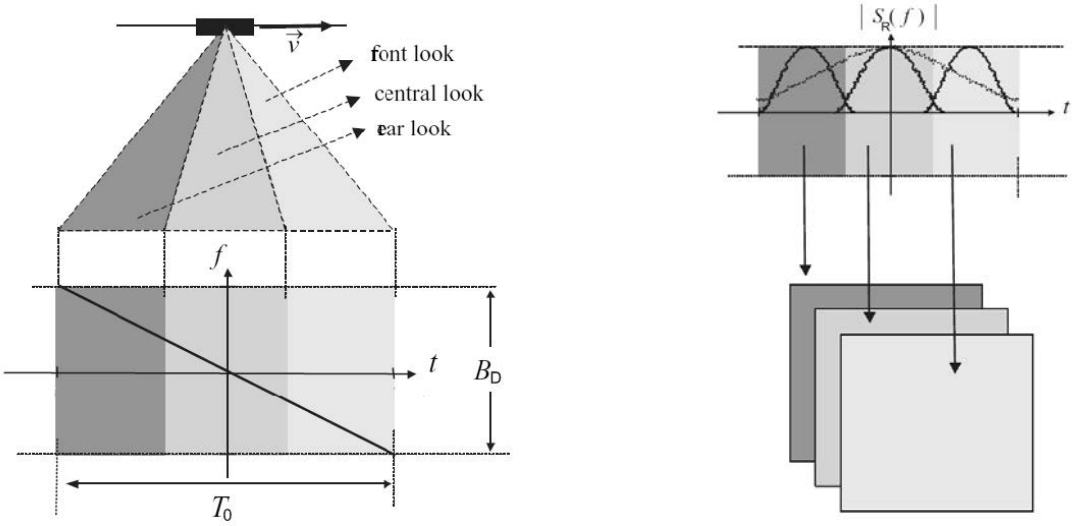

Fig. 1.18 - Multilooking principle: Doppler history (on the left) and incoherent summation (on the right).

1.4 SAR Impulse Response

A way to join both acquisition and image formation process, treating the SAR system from a more general point of view,it is to obtain the response of SAR system to a single point scatterer. In this way, a complete image, sometimes called reflectivity map, can be obtained by sums of the contributions of an arbitrary number of point targets. As said before, indicating with x, r respectively the azimuth and range direction, an ideal point target located at (x_0, r_0) should have an ideal impulsive response:

$$\sigma(x_0, r_0) = \sqrt{\sigma} e^{j\varphi} \delta(x - x_0, r - r_0) \tag{1.41}$$

where δ is the Dirac's function, φ the phase shift introduced by the target and σ is the complex radar cross section (RCS), which in general depends on the material, the imaging geometry, the wavelength and the polarization of the transmitted electromagnetic wave. Considering to transmit the general pulse with complex expression:

$$S_T(t) = p(t) e^{j(\omega_0 t + \psi(t))} \tag{1.42}$$

where $p(t)$ is the general window function for the amplitude and $\psi(t)$ is the general frequency modulation (or phase coding). The received signal will be:

$$S_R(t) = p_r\big(t - \tau(t)\big) e^{j[\omega_0(t-\tau(t)) + \psi(t-\tau(t))]} \tag{1.43}$$

with $\tau(t)$ the time variable delay and $p_r(t)$ the received amplitude attenuated by propagation and antenna pattern weighting. As we have previously said, considering the "start and stop" approximation, $\tau(t)$ can be considered constant inside each pulse and varying from pulse to pulse. In this case, considering $\tau_0 = 2r_0/c$, $p(t) = \text{rect}\left(\frac{t - T/2}{T}\right)$, and $\psi(t) = (K/2)t^2$, matching $S_R(t)$ with $S_T(t)$, we have:

$$\begin{aligned} S_R(t) &= \int_{-\infty}^{\infty} p_r(t-\tau_0) e^{j[\omega_0(t-\tau_0)+\psi(t-\tau_0)]}\ p(t+\tau) e^{-j(\omega_0(t+\tau)+\psi(t+\tau))} d\tau \\ &\approx \sqrt{\sigma} e^{j\varphi} e^{j\omega_0 t'} \frac{\sin\left[\frac{Kt'}{2}(T-|t'|)\right]}{\frac{Kt'}{2}(T-|t'|)} \frac{(T-|t'|)}{2} \mathrm{rect}\left(\frac{t'}{2T}\right) \\ &= \sqrt{\sigma} e^{j\varphi} e^{j\omega_0 t'} \mathrm{sinc}\left[\frac{Kt'}{2}(T-|t'|)\right] \frac{\mathrm{T}}{2} \mathrm{tri}\left(\frac{t'}{T}\right) \end{aligned} \tag{1.44}$$

with $t' = t - \tau_0$, $\mathrm{sinc}(x) = \sin(x)/x$, $\mathrm{tri}(x) = (1-|x|)\mathrm{rect}(x/2)$, and the gain losses due to the range attenuation and antenna pattern considered compensated. What Eq. (1.44) means is that around τ_0 we have a *sinc* function (due to the correlation between chirp pulses) multiplied with a *tri* function of duration $2T$ (due to the correlation between the *rect* of $p(t)$ and $p_r(t)$). Then, since the *sinc* function has the first zero value at:

$$t' \approx 2\pi/KT = 1/\Delta f \tag{1.45}$$

with Δf the chirp bandwidth, we can rewrite Eq. (1.44) as:

$$S_R(t) \approx \sqrt{\sigma} e^{j\varphi} e^{j\omega_0(t-\tau_0)} \mathrm{sinc}\left[\frac{KT}{2}(t-\tau_0)\right] = \sqrt{\sigma} e^{j\varphi} e^{j\omega_0(t-\tau_0)} \mathrm{sinc}[\pi\Delta f(t-\tau_0)] \tag{1.46}$$

Now, considering the change of coordinates $t = 2r/c$ (i.e. $\tau_0 = 2r_0/c$) and bring back the signal in base band, we have the point spread function (PSF) in range:

$$S_R(r) \approx \sqrt{\sigma} e^{j\varphi} e^{-j\frac{4\pi}{\lambda} r_0} \mathrm{sinc}\left[\pi \frac{(r-r_0)}{r_d}\right] \tag{1.47}$$

with the range resolution $r_d = c/2\Delta f$. Next, at the azimuth level we drop the hypothesis of "start and stop" approximation considering a time varying τ_0 due to the variable distance between the radar and the target during the motion. Then, considering a range migration correction, the r_0 inside the *sinc* function can be considered constant, whereas the phase term not. In particular, we have

$$S_R(r,t) \approx \sqrt{\sigma} e^{j\varphi} e^{-j\frac{4\pi}{\lambda} r_0(t)} \mathrm{sinc}\left[\pi \frac{(r-r_0)}{r_d}\right] \tag{1.48}$$

Next, writing $r_0(t) = \sqrt{r_0^2 + (vt)^2}$ and expanding in Taylor series around the time of approach:

$$r_0(t) \approx r_0 + (vt)^2/2r_0 \tag{1.49}$$

considering the azimuth point of approach x_0 at $t = 0$.Then, taking into account the antenna coefficient in azimuth $\beta\big(\theta(t)\big) = \beta(vt/r_0)$, with $\theta(t)$ the incidence angle from which the point target is seen by the antenna, the azimuth compression will be performed during the illumination time T_0 as:

$$\begin{aligned} S_R(r,t) &= \int_{-\frac{T_0}{2}}^{\frac{T_0}{2}} \beta\left(\frac{v\tau}{r_0}\right) S_R(r,\tau) e^{j\frac{4\pi}{\lambda} r_0(t-\tau)} d\tau \\ &= \sqrt{\sigma} e^{j\varphi} \mathrm{sinc}\left[\pi \frac{(r-r_0)}{r_d}\right] \int_{-\frac{T_0}{2}}^{\frac{T_0}{2}} \beta\left(\frac{v\tau}{r_0}\right) e^{-j\frac{4\pi}{\lambda}\left(r_0 + \frac{v^2\tau^2}{2r_0}\right)} e^{j\frac{4\pi}{\lambda}\left(r_0 + \frac{v^2(\tau-t)^2}{2r_0}\right)} d\tau \\ &= \sqrt{\sigma} e^{j\varphi} \mathrm{sinc}\left[\pi \frac{(r-r_0)}{r_d}\right] e^{j\frac{4\pi}{\lambda}\left(\frac{v^2}{2r_0}\right)t^2} \int_{-\frac{T_0}{2}}^{\frac{T_0}{2}} \beta\left(\frac{v\tau}{r_0}\right) e^{-j\frac{4\pi}{\lambda}\left(\frac{v^2}{r_0}\right)t\tau} d\tau \\ &= \sqrt{\sigma} e^{j\varphi} e^{-j\frac{4\pi}{\lambda}\left(\frac{v^2}{2r_0}\right)t^2} \mathrm{sinc}\left[\pi \frac{(r-r_0)}{r_d}\right] \frac{T_0}{2} \mathrm{sinc}\left[\frac{4\pi}{\lambda}\left(\frac{v^2}{r_0}\right) t \frac{T_0}{2}\right] \end{aligned} \tag{1.50}$$

where in the last equality we have presupposed a constant antenna coefficient $\beta(t) = 1$ (also called "rectangular aperture antenna") or an antenna pattern compensation. Now, since from Fig. 1.11 we can derive that $B_D/T_0 = 2v^2/\lambda r_0$, exploiting the equality $B_D = 2v/D$ we have:

$$T_0 = \frac{\lambda r_0}{Dv} \tag{1.51}$$

so that:

$$S_R(r,t) = \sqrt{\sigma} e^{j\varphi} e^{-j\frac{4\pi}{\lambda}\left(\frac{v^2}{2r_0}\right)t^2} \frac{\lambda r_0}{2Dv} \operatorname{sinc}\left[\pi \frac{(r-r_0)}{r_d}\right] \operatorname{sinc}\left[\frac{2\pi v t}{D}\right] \tag{1.52}$$

Finally, considering the coordinate change $x = vt$, with $x_0 = x|_{t=0}$, and expressing the azimuth resolution $r_{az} = D/2$, we have the final response:

$$S_R(r,x) = \sqrt{\sigma} e^{j\varphi} e^{-j\frac{4\pi(x-x_0)^2}{\lambda 2 r_0}} \frac{\lambda r_0}{2Dv} \operatorname{sinc}\left[\pi \frac{(r-r_0)}{r_d}\right] \operatorname{sinc}\left[\pi \frac{(x-x_0)}{r_{az}}\right] \tag{1.53}$$

which gives the following PSF $h(r,x)$ of the system:

$$h(r,x) = e^{-j\frac{4\pi x^2}{\lambda 2 r_0}} \frac{\lambda r_0}{2Dv} \operatorname{sinc}\left(\pi \frac{r}{r_d}\right) \operatorname{sinc}\left(\pi \frac{x}{r_{az}}\right) \tag{1.54}$$

that is often expressed as:

$$h(r,x) \approx \operatorname{sinc}\left(\pi \frac{r}{r_d}\right) \operatorname{sinc}\left(\pi \frac{x}{r_{az}}\right) \tag{1.55}$$

presupposing the phase term due to the target and the amplitude term corrected by calibration. Therefore, PSF of the SAR system can be considered ideally equal to that of a filter with rectangular bandwidth of sides $2/D$ in azimuth frequency and $2\Delta f/c$ in range one.

1.5 SAR System Constraints and Ambiguities

While the radar is moving, it is interesting to note the instantaneous situation of the acquired points on the ground. Naturally, the radar should be able to distinguish between points at different range and equal Doppler frequency (radial velocity) or, conversely, between points at equal range but with different Doppler frequency. Nevertheless, in an ideal situation where the radar points its antenna directly under itself, there would be ambiguity points (see Fig. 1.19(a)). Thus, one of the reasons to have a side-looking acquisition (other than improving ground range resolution) is to solve the possible ambiguities among acquired points (see Fig. 1.19(b)).

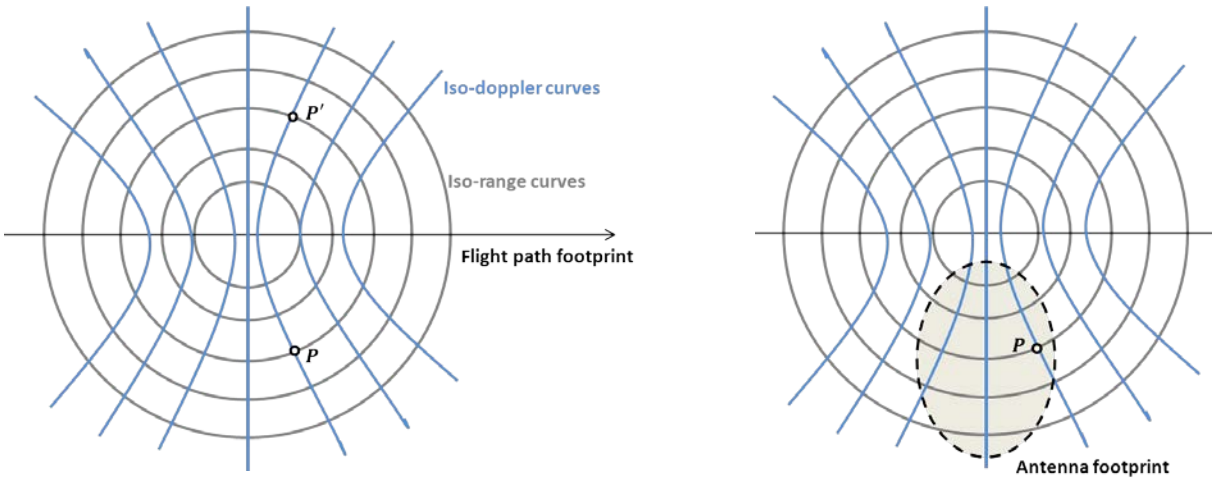

(a) (b)

Fig. 1.19 - Ambiguous points on the same iso-range and iso-doppler curves.

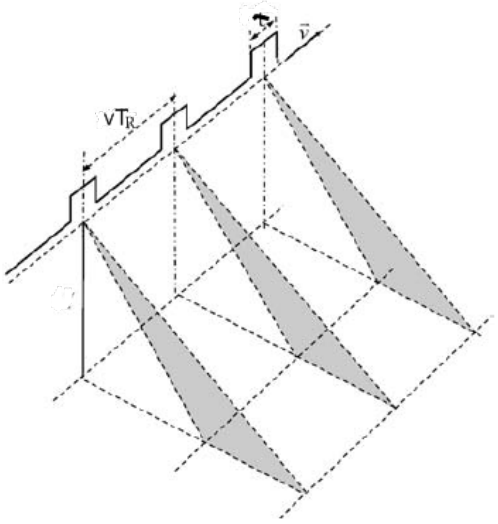

Fig. 1.20 - Block diagram of the range-Doppler focusing algorithm.

However, even avoiding these kinds of ambiguities, there are other constraints we have to respect to design an accurate SAR system. For example, each time a pulse is transmitted in azimuth direction, we receive the signal in Eq. (1.16) whose frequency bandwidth B_D spans from $-f_{D_M}$ to f_{D_M} (see Fig. 1.11).

Clearly, the **maximum Doppler frequency** f_{D_M} is due to the points at the extremities of the antenna footprint in azimuth (see Fig. 1.21). This implies that, since the Doppler frequency is defined as:

$$f_{D_M} = \frac{2v_r}{\lambda} \tag{1.56}$$

with v_r the radial velocities of the extreme points:

$$v_r = v\cos\vartheta = v\cos\left(\frac{\pi}{2}-\frac{\beta_{az}}{2}\right) = v\sin\left(\frac{\beta_{az}}{2}\right) \approx v\frac{\beta_{az}}{2} \tag{1.57}$$

Exploiting Eq. (1.2), we retrieve:

$$f_{D_M} = \frac{v\beta_{az}}{\lambda} = \frac{v}{D} \tag{1.58}$$

Now, indicating with T_R the period of pulse transmission ($PFR = 1/T_R$), it becomes clear that to avoid aliasing the following relation has to be respected:

$$PRF \geq 2f_{D_M} = \frac{2v}{D} \tag{1.59}$$

Finally, since vT_R is the space covered by the radar between two subsequent retransmissions, we can rewrite Eq. (1.59) as:

$$vT_R \leq \frac{D}{2} = r_{az} \tag{1.60}$$

with r_{az} the azimuth resolution of the SAR. Therfore, if we wanted to improve the resolution decrising D, we would have to raise the pulse repetition frequency PRF (or dim T_R).

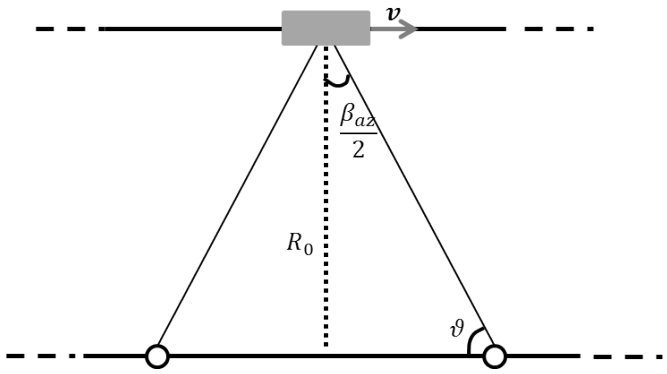

Fig. 1.21 - Extreme points in the azimuth footprint (indicated with white circles) have the maximum Doppler frequency.

Furthermore, considering the reception in time of the transmitted pulse, it is clear that before transmitting a new pulse, we have to wait the reception of the whole signal, that is (see Fig. 1.22):

$$T_R > \frac{2R_{far}}{c} \tag{1.61}$$

where $R_{far} = R_{near} + \Delta R$. Consequently, considering Eq. (1.59) and (1.61), the PRF has two different constraints:

$$2f_{D_M} = \frac{2v}{D} \geq PRF < \frac{c}{2R_{far}} \tag{1.62}$$

Nevertheless, exploiting geometrical consideration, even the rightmost part of Eq. (1.61) can be linked to the physical dimension of the antenna in range W. In fact, considering the following equations:

$$\tan\theta \approx \frac{\Delta R}{R_{near}\beta_r};\ R_{near} \approx \frac{h}{cos\theta};\ \beta_r \approx \frac{\lambda}{W} \tag{1.63}$$

we have:

$$\Delta R = \tan\theta\, R_{near}\beta_r = \tan\theta \frac{h}{cos\theta}\beta_r = \tan\theta \frac{h\lambda}{Wcos\theta} \tag{1.64}$$

therefore the **PRF constraint**s become:

$$2f_{D_M} = \frac{2v}{D} \geq PRF < \frac{c}{2R_{far}} = \frac{c}{2(R_{near} + \Delta R)} = \frac{c(cos\theta)}{2h\left(1+\frac{\lambda}{W}\tan\theta\right)} \tag{1.65}$$

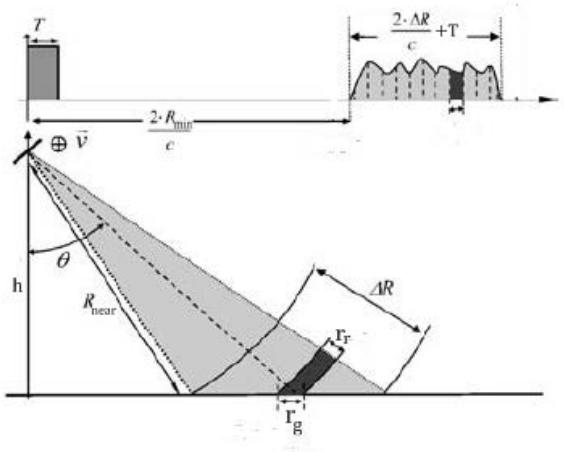

Fig. 1.22 - Transmission and reception in range sight.

1.6 Other Acquisition Modes: Spotlight and Scansar

The imaging mode descripted until now, which is obtained by pointing the antenna along a fixed direction with respect to the flight platform path, is the so called **Stripmap mode**. However, in this operating mode, if we wanted to improve azimuth resolution we would reduce the length D of the antenna so that the PRF has to be increased and, to avoid range ambiguity, the acquired swath has to be reduced by increasing the antenna height W (Eq. (1.65)). To maintain the antenna dimensions and changing at the minimum the swath size, the idea is to steer the antenna pattern (both in the azimuth and the elevation plane) during the overall acquisition time in order to illuminate the required scene for a time period longer than the one of the standard Stripmap mode. In this way, the length of the synthetic antenna is increased and consequently the azimuth resolution is raised (at expense of the azimuth coverage). This acquisition procedure is commonly known as **Spotlight mode** (see Fig. 1.23), recalling the way an actor is followed across the stage by a theatre spotlight.

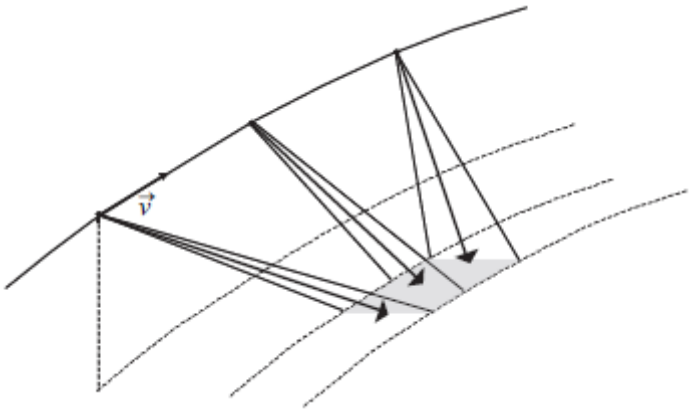

Fig. 1.23 - Spotlight mode principle.

What happens at the analytical level is that the Doppler band of the received signal is a little increased but it is still compatible with the previous PRF value. Nevertheless, differently from the Stripmap mode, at each reception the reference point at the center of the antenna footprint will have a time variable Doppler reference due to the variable azimuth angle of acquisition, which is also called skew angle (see Fig. 1.24). The disadvantage of Spotlight mode is that it does not allow continuous acquisition in azimuth direction. In fact, while in Stripmap mode very long subsequent swaths can be recorded, in Spotlight mode the antenna pointing has to be reset, so to avoid such type of acquisition.

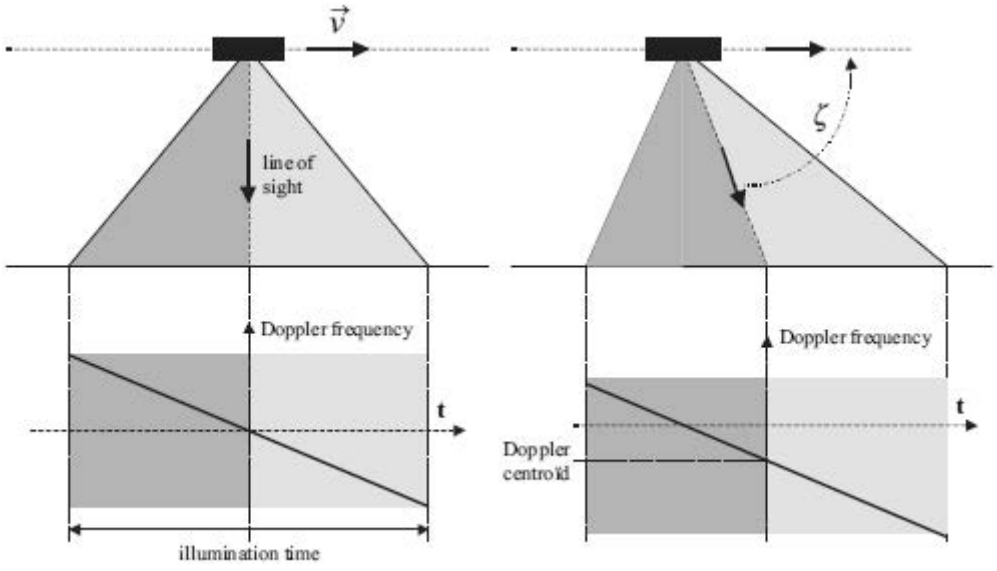

Fig. 1.24 - Shift of the Doppler centroid due to the acquisition by a skew angle.

An opposite reasoning from that helpful to pass from Stripmap mode to Spotlight mode has to be done to pass from the former to the so called **Scansar mode**. In fact, in Scansar mode the goal is to acquire a wider range swath without the need to change antenna dimensions. The solution is to step periodically the antenna beam to neighboring sub-swaths (see Fig. 1.25). Inevitably, the azimuth resolution is reduced by a factor equal to the number of sub-swath acquired since only a fraction of the synthetic antenna length is available in azimuth for each sub-swath.

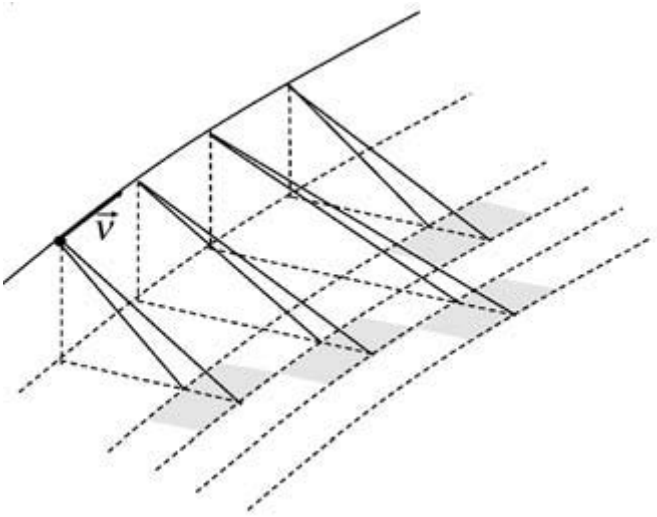

Fig. 1.25 - Scansar mode principle.

1.7 Satellite SAR Systems

Satellite SAR systems are a very important class of SAR systems that enable earth observation to be performed routinely. Usually, satellite systems are designed to have near-polar orbits (i.e. the satellite passes close to both poles as it orbits the globe) to ensure nearly global coverage. As for altitude, most of them operate at around 600-800 km. They are often sun-synchronous and, even though this requirement is mainly useful for optical remote sensing satellites, it can be exploited by SAR satellites to keep a fixed orientation of their solar panels. Usually, among the numerous parameters characterizing the satellite orbit, only a subset should be known in order to have an adequate system understanding:

- **Orbit direction**: it is said *ascending* when the satellite crosses the equator going to North, whereas is said *descending* when it goes to South (see Fig. 1.26)

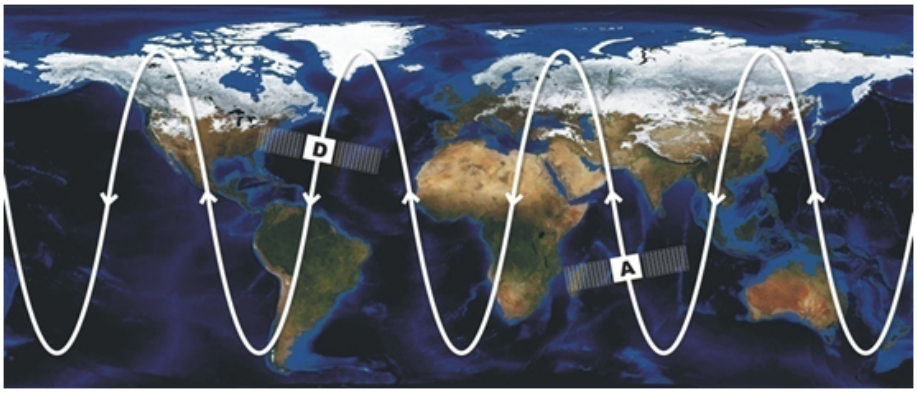

Fig. 1.26 - Orbit directions: "A" indicates ascending and "D" descending.

- **Orbit inclination**: it is the angle between the equatorial plane and the orbital plane when the satellite move in ascending direction (see Fig. 1.27). For example, CSK system has nominal inclination orbit of 97.86°.

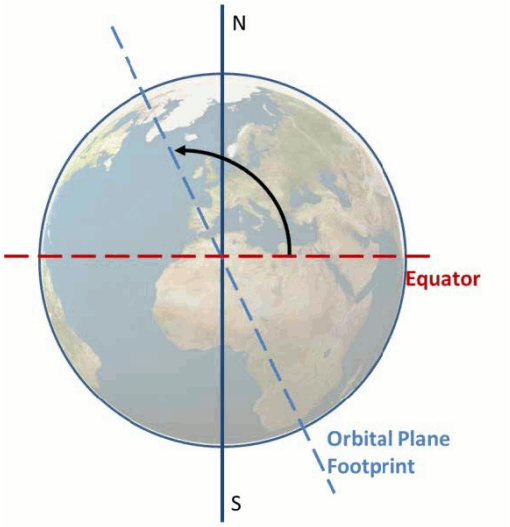

Fig. 1.27 - Orbit Inclination.

- **Look side**: it can be *right* or *left* and, given the projection of the orbital plane on the ground, it indicates in which part of the earth the radar acquires the data (see Fig. 1.28).

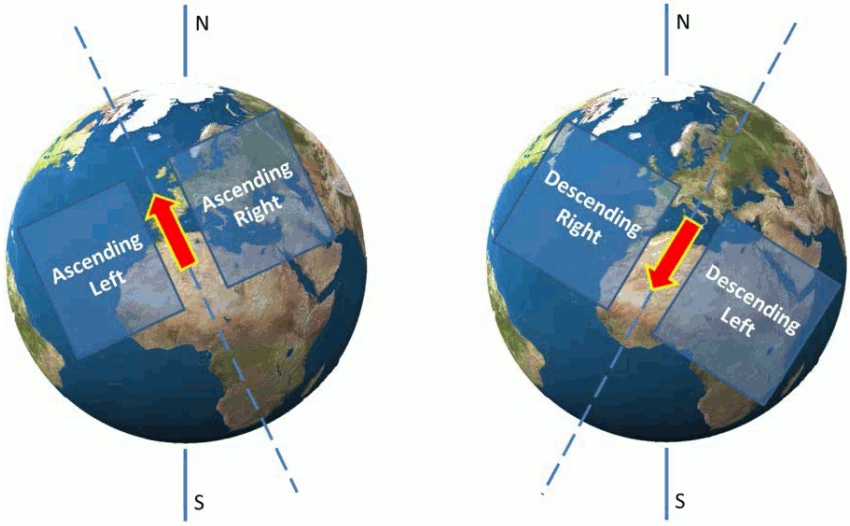

Fig. 1.28 - Look side reference.

- **Eccentricity**: it characterizes the elliptic shape of the orbit and it is computed as

$$e = \sqrt{s_M^2 - s_m^2 / s_M^2} \tag{1.66}$$

where s_m^2 and s_M^2 are the semi-minor and semi-major axis of the ellipse. Since the orbits are very near to a circle, it is usually very small. For example, CSK system has $e = 0.00118$.

- **Revolution Period**: it is the time the satellite needs to compute a complete round of the orbit and, presupposing an ideal circular orbit, can be only expressed as function of geometrical parameters only. In fact, indicating with R_e the earth radius, h the radar altitude and g the gravity acceleration at the earth level (i.e. $g = GM/R_e^2$ with G the gravitational constant and M the earth mass) and taking into account that, in order to maintain the orbit, the centripetal force $F = v/(R_e + h)^2$ due to the orbital velocity has to be equal to the gravitational force $F = GM/(R_e + h)^2$, the orbital velocity can be expressed as

$$v = \sqrt{R_e^2\, g/(R_e + h)} \tag{1.67}$$

Therefore, the revolution period becomes

$$T = 2\pi(R_e + h)/v = 2\pi\sqrt{(R_e + h)/R_e^2 g} \tag{1.68}$$

For example, for CSK satellite constellations, using these approximated formulas and considering $R_e = 6378\,\text{km}$, $h = 619.6\,\text{km}$, $g = 9.80665\,m/s^2$, we have $v \approx 7550\,m/s$ and $T \approx 97\,min$ (i.e. 14.8373 revolutions at day), which are very near to the nominal values (14.8125 revolutions at day).

- **Orbit Cycle**: Period of time an area can be acquired with the same geometry, e.g. CSK system has a cycle of about 16 days.

Nevertheless, real system are sometime far from the ideality behavior descripted so far. For example, mainly due to atmospheric turbulence (less marked in the spaceborne system than in airborne one), deviations of the trajectory from the nominal one as well as altitude and forward velocity variations frequently occur. In fact, to compensate these geometric and radiometric resolution losses, specific modifications on the ideal processing have to be done. In general, error corrections in processing can be performed through flight information available at the raw data processing stage provided by inertial navigation units (INU) and Global Positioning System (GPS) mounted on-board the system. Alternatively, many techniques exist to compensate motion errors by a direct estimation of them from the raw data (e.g. Autofocusing) [1]. Moreover, in the previous discussions we have presupposed to know exactly the Doppler shift of point targets located on the ground throughout the use of acquisition geometry and aircraft velocity. However, to compute such a term, even the rotation velocity of the earth has to be taken into account. For example, satellite system in ascending direction that wanted to have a perpendicular pointing should skew their antenna slightly forward to compensate such radial velocity component. Finally, in the case of a space borne system, the hypothesis to transmit and receive the impulse in the same position ("start-stop hypothesis") is no longer valid. In fact, considering an observation range $R_0 = 900km$ (e.g. the CSK system with incidence angle of about 47°) and a satellite velocity $v = 7000\ m/s$, the radar receive the transmitted pulse after $6\,ms$, i.e. after covering a distance of $42\,m$. Therefore, the return time is so great that the echo received just after the pulse transmission does not come from the corresponding pulse but from one that was transmitted several cycles earlier. For the CSK satellite, a typical $PRF = 4000\,Hz$ corresponds to a transmission period $T_R = 250\,\mu s$, i.e. the echo of the first pulse transmitted is received around the transmission of the pulse twenty-fourth. Therefore, the approximation violation has to be taken into account in the azimuth compression, whereas due to the high value of R_0 with respect to the distance covered by the radar before receiving, the phase shift in range could be considered nearly negligible.

1.8 Geometrical Effects on Acquired Images

From a general point of view, SAR systems remotely take electromagnetic measurements on range direction. This operating way generates some "distortions" when we use the acquired images to take distance measurements between points on the ground. The effects of this "range vision" are more marked on regions characterized with different elevation levels (e.g. mountains, hills, urban areas, etc.) and they have to be taken absolutely into account when any measurement is picked up from SAR images.

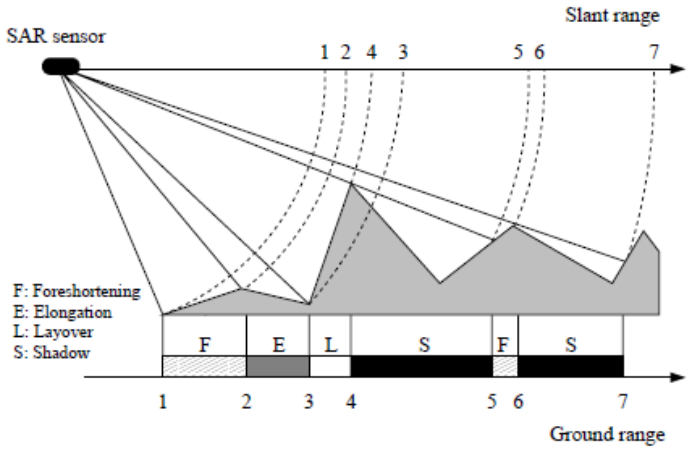

Fig. 1.29 - Geometrical distortions due to the radar "range vision".

In Fig. 1.29 are shown the main geometrical distortions that characterize SAR acquisition:

- **Foreshortening**: it refers to the fact that two points at different level of elevation can have a very short range distance in the acquired image. Then, since the received energy comes from a more extended area with a steeper inclination than flat areas, the image pixel has a higher amplitude (see points 1 and 2 in Fig. 1.29).

- **Layover**: it is an extreme case of foreshortening and it refers to the fact that a point at the top of a mountain may be closer to the radar with respect to its bottom (see points 3 and 4 in Fig. 1.29). Therefore, in the acquired image the positions of the top and bottom points are inverted with respect to their ground range coordinates. In this case, the amplitude of the acquired pixel is greater than in the standard foreshortening case.

- **Elongation**: it is the reverse case of foreshortening, where downhill zones appear longer than in the ground range coordinates and the corresponding pixel appear darker than usual.

- **Radar Shadow**: It is due to the absence of received signal from areas that are not illuminated by the radar. Clearly, they are characterized by the lowest amplitude values of the corresponding pixels in the image.

Naturally, as reported in Eq. (1.4), given a fixed range resolution r_r, the ground range resolution r_g on a plain area can be computed exploiting the local incidence angle ϑ of the acquired range cell as:

$$r_g = \frac{r_r}{\sin\vartheta} \tag{1.69}$$

Nevertheless, not only will the ground range resolution vary from near range to far range, but also it will strongly depend on the topography of the acquired scene.

1.9 Real SAR Data

The methods devised and presented in this document are evaluated on different real SAR data (other than simulated ones). A list of the reported real SAR data is summarized in this section.

1.9.1 MSTAR Images

These data belong to the public dataset aviable by the Moving and Stationary Target Acquisition and Recognition (**MSTAR**) program, and in particular to the **CLUTTER** dataset. These images are acquired in 1995, near Redstone Arsenal (Alabama,USA), by an airborne SAR sensor developed by Sandia National Laboratory (SNL) in partnership with the Defense Advanced Reaserch Projects Agency (DARPA) and the Air Force Research Laboratory (AFRL). The main image properties are listed in Tab. 1.1. Even though the MSTAR dataset contain images with military thanks too, in the rest of the document with MSTAR we always refer to the CLUTTER dataset. In Fig. 1.30 we can see some examples of images belonging to the MSTAR dataset. As can be seen from these image samples, the MSTAR dataset contains images acquired in rural areas.

Range resolution	0.304700 m
Cross-range resolution	0.304700 m
Range pixel spacing	0.202148 m
Cross-range pixel spacing	0.203125 m
Additive noise	-32 to -34dB
Center frequency	9.60 GHz
Bandwidth	0.591GHz
Dynamic range	64 dB
Azimuth beamwidth	8.8 °
Elevation beamwidth	6.8°
Polarization	HH
Bits per pixel	16

Tab. 1.1 - Technical properties of the MSTAR images.

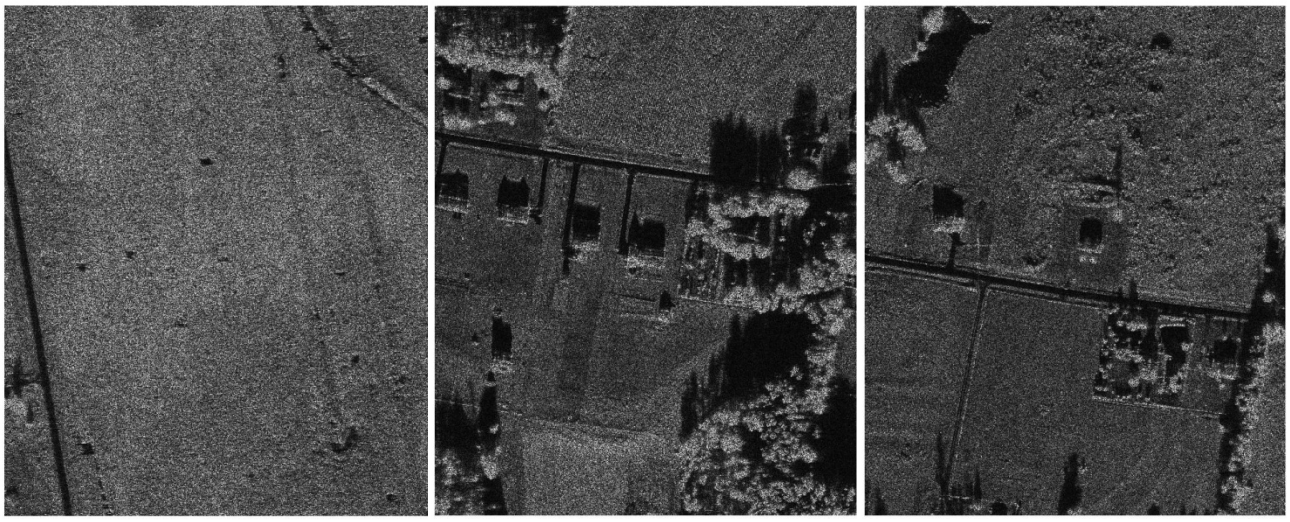

(a) (b) (c)

Fig. 1.30 - Examples of images belonging to the CLUTTER MSTAR dataset. (a) Image "HB06173". (b) Image "HB06210". (c) Image "HB06212".

1.9.2 CSK Images

The CSK images reported in this document belong to different CSK products and, without other specification, they will be referred by their name. It is worth noting that the entire images reported are **provided by courtesy of italian space agency (ASI)**.

1.9.2.1 CSK1

The images in Fig. 1.31, which depicts an airport, has been acquired in Spotlight 2 mode with polarization **HH** and incidence angle near/far of **55.9°/56.3°** and has a theoretical equivalent number of look equal to **1**. It is a CSK **L1B product**, i.e. it is in ground range-azimuth coordinates.

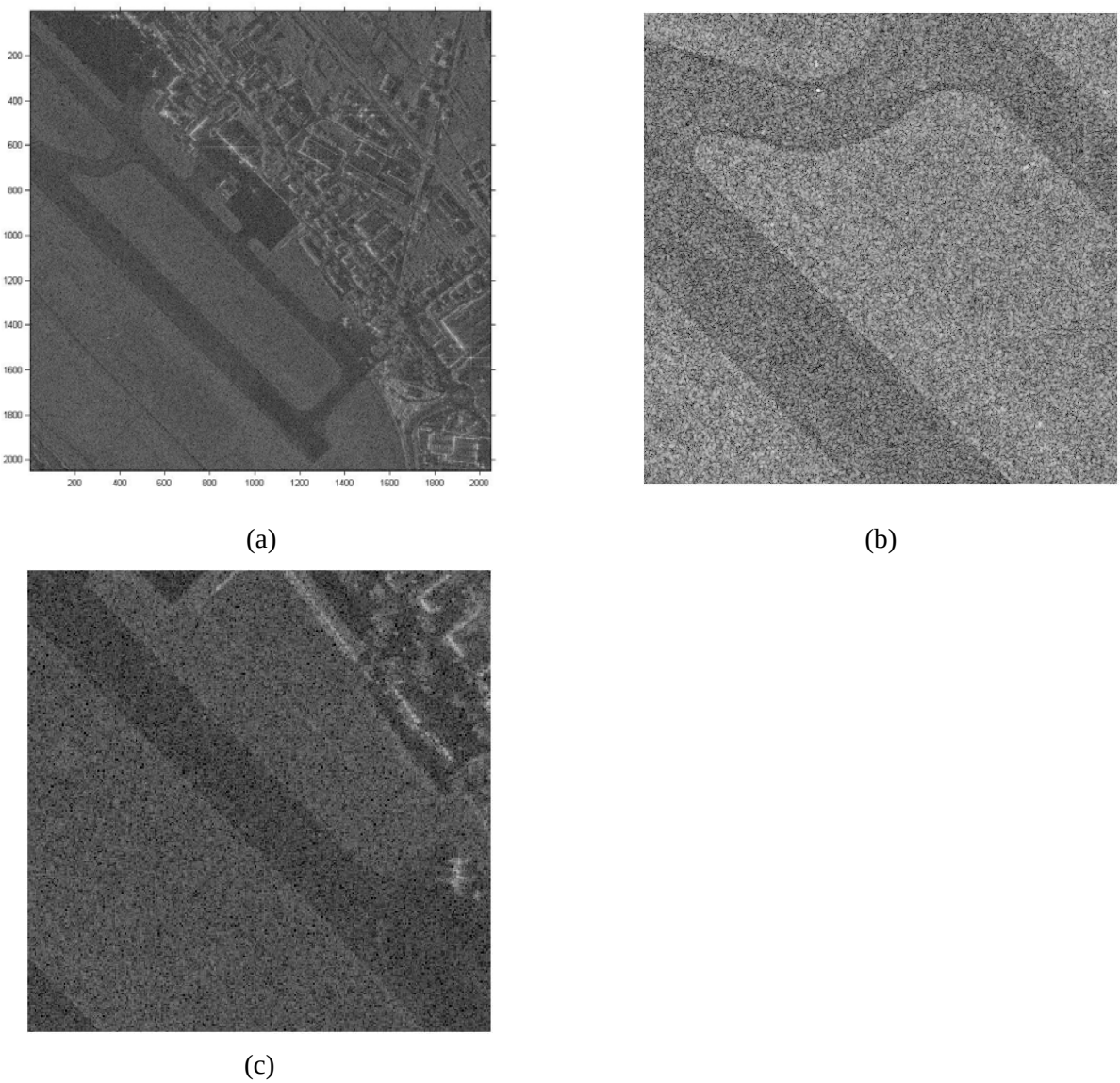

(a) (b)

(c)

Fig. 1.31 - (a) Amplitude of "CSK1" image. (b) Runway detail (512x512 px). (c) Airport detail (512x512 px).

1.9.2.2 CSK2

The image in Fig. 1.32, which depicts an airport, has been acquired in Spotlight 2 mode with polarization **HH** and incidence angle near/far of **51.1°/51.5°** and has a theoretical equivalent number of look equal to **1**. It is a CSK **L1B product**, i.e. it is in ground range-azimuth coordinates.

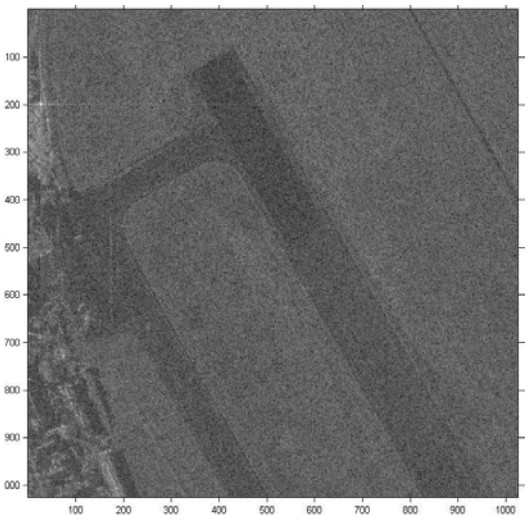

Fig. 1.32 - Amplitude of "CSK2" image.

1.9.2.3 Others

The image in Fig. 1.33, which depicts an airport, has been acquired in Spotlight 2 mode with polarization **HH** and incidence angle near/far of **23.9°/24.8°** and has a theoretical equivalent number of look equal to **1**. It is a CSK **L1A product**, i.e. it is in slant range-azimuth coordinates.

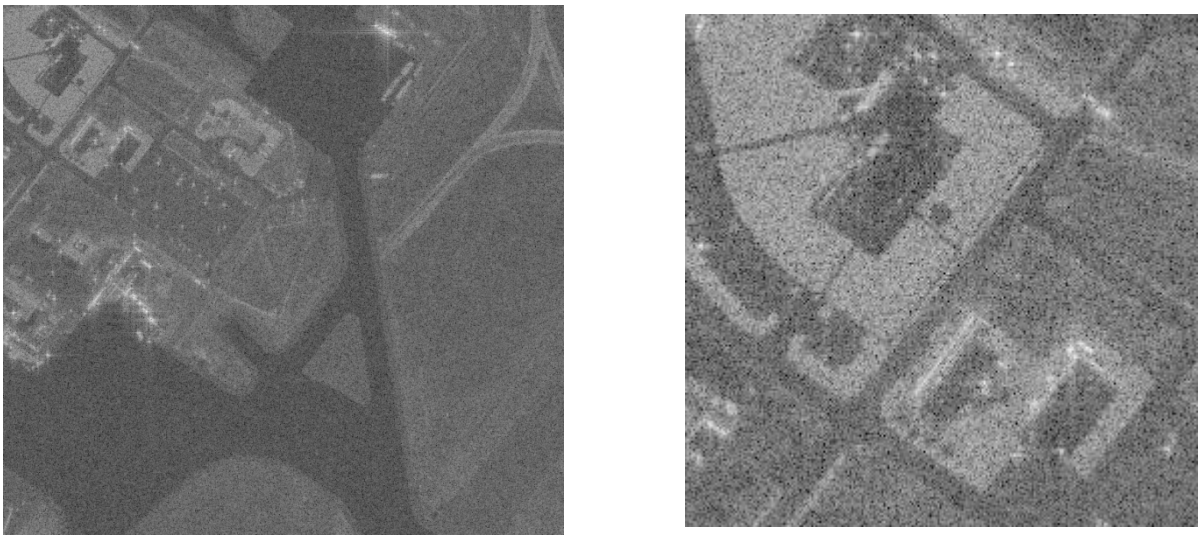

(a) (b)

Fig. 1.33 - (a) Amplitude of "Tucson" image. (b) Small detail (256x256 px).

The images in Fig. 1.34, which depicts the same airport, has been acquired in Spotlight 2 mode with polarization **HH** and different incidence angle. They are CSK **L1C product**, i.e. they are geo-located on the reference ellipsoid, and they have a theoretical equivalent number of look equal to **1**.

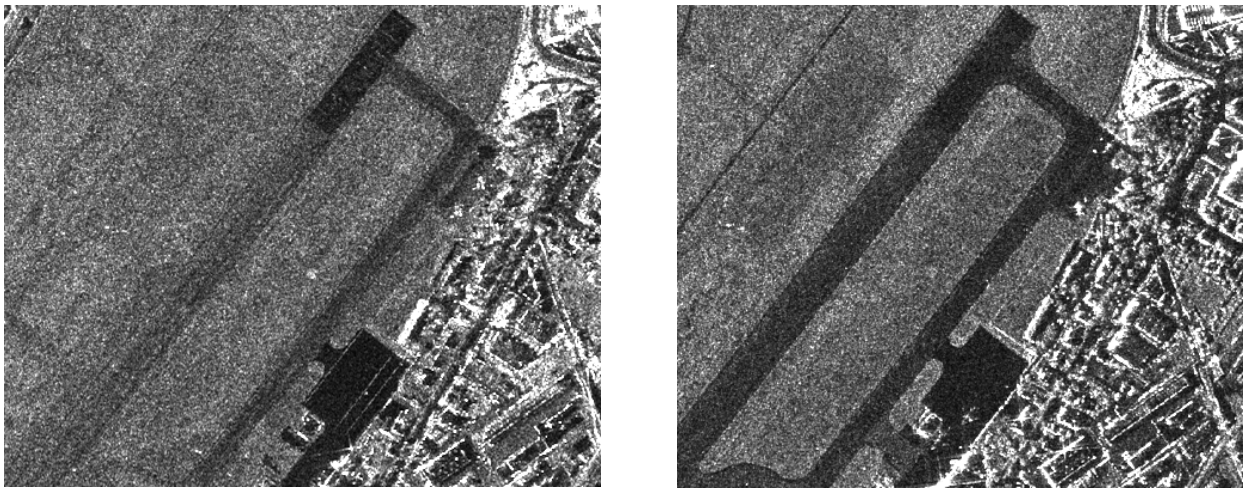

Fig. 1.34 - (a) Amplitude CSK image with incidence angle near/far 26.5°/27.4°. (b) Amplitude CSK image with incidence angle near/far 55.9°/56.3°.